CHARACTERIZATION OF SOCCER BALL PARAMETERS FOR THE

MANUFACTURING OF PROTECTIVE HEADBANDS AND THE FREQUENCY

DOMAIN EVALUATION OF FOOTBALL HELMETS

A Thesis

Submitted to the Faculty

of

Purdue University

by

Nicolas Leiva

In Partial Fulfillment of the

Requirements for the Degree

of

Master of Science in Biomedical Engineering

May 2019

Purdue University

West Lafayette, Indiana

THE PURDUE UNIVERSITY GRADUATE SCHOOL
STATEMENT OF THESIS APPROVAL

Dr. Eric A. Nauman, Chair

    School of Mechanical Engineering

Dr. Thomas M. Talavage

    School of Electrical and Computer Engineering

Dr. Scott Lawrance

    College of Health and Kinesiology

Approved by:

    Dr. George R. Wodicka

        Dane A. Miller Head of Biomedical Engineering

Dedicated to my mom, dad and brother back home in Colombia. Their unflagging support during these past two years was vital for the completion of this project. I hope to make them proud.

ACKNOWLEDGMENTS

I would like to start off by acknowledging Dr. Nauman. If it were not for him, I would not have understood the true meaning of research or what being properly mentored feels like. It has been an adventure to learn from a world-class researcher. I would be lucky to be one fifth of the investigator he is. Dr. Talavage and Dr. Lawrance, thank you for showing me what hard work can achieve and keeping me motivated to help athletes through research.

To all the members of the HIRRT Lab: thank you. Every single one of you contributed to this work, whether you noticed or not. A special shout-out goes to Kevin, Mike, Roy and Taylor who were always willing to drop knowledge on me and give me work-related advice. Not to mention, Bre-Bre, Sean, Patrick, Sadid, Jacob and Leora who kept me smiling through the entire process. You guys are the real MVPs.

Non-work related, a special thank you goes out to the members of the Purdue Mens Rugby Club. You guys kept me sane. Asimismo, un especial agradecimiento a mi comunidad Colombiana, que me hicieron sentir en casa en los momentos que mas lo necesitaba. En especial a Kike, Edu, Marti y Aleja, que fueron mi familia durante estos dos aos. Por ultimo, le quiero agradecer a Don Cuervo, por ensearme el verdadero significado de la dedicacion.

TABLE OF CONTENTS

LIST OF TABLES

LIST OF FIGURES

SYMBOLS

n_d	number of variables of interest for dimensional analysis
k	number of base quantities needed to describe variables in dimensional analysis
F_p	peak impact force
v	incoming ball velocity
p	inflation pressure of soccer ball
d	diameter of soccer ball
m_b	mass of soccer ball
L	base quantity for length
M	base quantity for mass
T	base quantity for time
Π	pi-group for dimensional analysis
B	coefficient for dimensional analysis under intermediate asymptotic assumption
β	coefficient for dimensional analysis under intermediate asymptotic assumption
n_p	number of level factors for Cotter's method
C_o	odd contrast for Cotter's method
C_e	odd contrast for Cotter's method
y	output value of trial for Cotter's method
M_{CM}	measure calculated for Cotter's method
S_{CM}	sensitivity index calculated for Cotter's method
a_p	peak linear acceleration
$\ddot{\theta}_p$	peak angular acceleration

$\int F(t)dt$	impulse derived
m_H	mass of the head
m_T	total mass of the H3 system
w_n	width of the neck
L_n	length of the neck
t^*	time scaling factor
t_r	reference time
Δt	time of impact
$T(\omega)$	transmissibility
HD	head
HT	helmet
$\ddot{X}(\omega)$	acceleration in frequency domain
$F(\omega)$	force in frequency domain
$H(\omega)$	frequency response function
$X(\omega)$	displacement in frequency domain
k_{HT}	spring constant of helmet system
c_{HT}	damping coefficient of helmet system
x	displacement in time domain
$\dot{x}$	velocity in time domain
f	velocity in time domain
$Z(\omega)$	mechanical impedance
G_{XY}	cross spectral density
G_{XX}	auto spectral density

ABBREVIATIONS

TBI	traumatic brain injury
CTE	chronic traumatic encephalopathy
NOCSAE	National Operating Collegiate on Standards for Athletic Equipment
FIFA	Fédération Internationale de Football Association
NCAA	Nacional Collegiate Athletic Association
TPU	thermoplastic polyurethane
PSI	pound-force per square inch
PLA	peak linear acceleration
CVR	cerebrovascular reactivity
MR	magnetic resonance
PTA	peak translational acceleration
PAA	peak angular acceleration
ANCOVA	analysis of covariance
CF-6	carbon fiber six layer
ASTM	American Society for Testing and Materials
FROI	frequency range of interest
FRF	frequency response function
HAE	head acceleration event
CoM	center of mass
FFT	fast Fourier transform

ABSTRACT

Leiva, Nicolas M.S.B.M.E., Purdue University, May 2019. Characterization of Soccer Ball Parameters for the Manufacturing of Protective Headbands and the Frequency Domain Evaluation of Football Helmets. Major Professor: Eric A. Nauman.

An increase of 153,375 to 248,418 traumatic brain injuries (TBI) due to incidents in sports and recreation activities has been reported in the past couple of years in the US alone. These are grounds for concern for athletes partaking in sports with a high incidence of TBIs such as football and soccer. The latter, traditionally not classified as a contact-sport, has attracted research due to participants using their head as an instrument for heading. Voluntary heading, in combination with lenient laws and regulations concerning TBI expose how soccer players are easily at risk of injury. On the other hand football, an aggressive sport by nature, has brought attention to the possible neurocognitive and neurophysiological ramifications of repetitive subconcussive impacts. One of these is in the form of a progressive neurodegenerative pathology known as chronic traumatic encephalopathy (CTE). A priori reasons revealed, led to a need to characterize the most important variables involved in ball-player interactions within soccer simulated gameplay. By understanding these, it would be possible to obtain parameters to design and manufacture new composite-material based protective headgear unlike products that are commercially available nowadays. In addition, development of a testing protocol focused on frequency domain variables - transmissibility and mechanical impedance - would allow to evaluate the performance of football helmets. A focus would be set on low impacts categorized as subconcussive impacts. Incoming velocity and inflation pressure were identified as the most influential variables affecting the peak impact force of a soccer ball. An innovative 6-layer carbon fiber headband, with silicone padding, was manufactured that out-performed existing

headgear at attenuating peak linear acceleration. Lastly, quantification of the transmissibility and mechanical impedance indicated poor performance of football helmets below 60 Hz.

1. INTRODUCTION

1.1 Motivation

Increasing concern in the risk of athletes experiencing traumatic brain injury (TBI) has led to a surge of interest from traditional media and researchers in the medical and engineering field. In the United States alone, an increment of 153,375 to 248,418 was observed in the number of visits emergency departments received due to TBI related incidents in sports and recreation activities [1]. Taking into account that participation in sport is increasing, it is expected that the amount of TBI is set to grow as well [2]. According to the Center of Disease Control (2011) the principal diagnosis of these injuries was *concussion*. The International conference of concussion in sport held in 2017 defined sport related concussion as "*a traumatic brain injury induced by biomechanical forces.*" [3]. Some of the tools/mechanics used to help describe and diagnose these injuries are a direct blow to the head; short-lived neurological impairment that should resolve over a brief period of time; neuropathological alterations that are not necessarily detected through neuro-imaging; and possible prolonged signs and symptoms [3].

Nonetheless, recent studies have shown that despite not being clinically diagnosed with a sport related concussion, athletes partaking in sports still suffer neurocognitive [4] [5] and neurophysiological consequences [6] [7] [8]. A clear pathology exemplifying these asymptomatic alterations is chronic traumatic encephalopathy (CTE) [9]. A pathology that is associated to progressive neurodegeneration that can ultimately lead to mood alterations and nuerocognitive impairments [10]. An example of sports that have been linked to CTE are soccer [11] and American Football [12].

The former, is not necessarily classified as a contact sport, albeit, existing studies have shown a high incidence of TBI incidents in soccer players amongst other tradi-

tional contact sports [13] [14]. The use of the head is an essential aspect of the game, given that it can be used to shoot, control, pass and defend the ball. Nonetheless, it is rendered a double-edged sword since these athletes are being subjected to high number of subconcussive impacts [15] [16]. Moreover, little is known about how different variables affect the resultant force experienced during collisions between the head and other objects in the field. Whether it is a soccer ball, another player or the ground. Hence, the design of existing protective headgear is not tailor-made to mitigate the possible range of impact forces registered in a game [17].

On the other hand, football is highly associated to TBI [18] [19] [20] thanks to the aggressive nature of the game. In contrast to what is seen in soccer, protective headgear is a requirement in the sport for more than half a century (Levy, 2004). As a consequence an evolution in helmet design and its posterior evaluation and certification is natural. However, conventional certification programs such as those offered by the National Operating Collegiate on Standards for Athletic Equipment [21] lack specific attention to the repetitive subconcussive episodes that result in long-term neurocognitive damage.

1.2   Study Objectives

This first objective of this thesis is to characterize the velocity profile of soccer balls by simulating in-game header impacts. The goal was to determine how to alter the mass and pressure of a soccer ball in order to reduce the peak force felt during impact. The second objective was to design, manufacture and evaluate new personal protective headgear for soccer. Lastly, the final objective consisted in developing evaluation criteria for the performance of protective headgear through modal analysis.

2. HEADING A SOCCER BALL AND THE CHARACTERIZATION OF PARAMETERS THAT INFLUENCE ITS PEAK IMPACT FORCE

††

2.1 Motivation

Bearing in mind that soccer has more than 270 million people active worldwide [22] and more than 16 million registered players solely in the United States [15] player's health and safety is non-negotiable. To the untrained eye, soccer is usually not classified as a risk-related activity that can lead to TBI [23]. Nonetheless, it has been categorized as a contact sport [24] [25] [26]. The natural aggression within the sport undeniably ushers athletes to sustain head injuries across different levels of play, whether youth, college or elite/professional. More so, several studies have shone a light on the fact that athletes involved in soccer are at higher risk of head injury per player when compared to other contact sports [27] [13] [28].

Varied mechanisms of acquiring TBI are linked to soccer players, including player to player collisions [16], heading the ball during open-play [15] [16] [29], contact between players and the ground [27] [13] and even position-specific situations such as goalkeeping [13]. In spite of the variety of mechanisms, when utilizing one's head as an instrument during game play - whether its for passing, shooting or controlling the ball - [15] an athlete can experience accelerations up to a range of $18 - 25Gs$ [30]. The resulting acceleration can be influenced by a series of factors, including the velocity of the soccer ball or the pressure at which it was inflated [31] [29]. Pressure of the soccer ball is a factor that is regulated by governing entities such as the National Col-

---

††Content from this chapter is currently under revision: Auger et al., manuscript in preparation

legiate Athletic Association (NCAA) and the Fédération Internationale de Football Association (FIFA), leaving little leeway for modification by athletes. The ranges established are $8.5 - 16.21$ PSI and $8.5 - 16$ PSI respectively for colleges in USA [32] and active players worldwide [33]. Velocity-wise, soccer balls have been registered to surpass the 30 m/s mark (67 mph) across different levels of play [?] [34] [35] [36].

In furtherance of the possibility of characterizing parameters within active game-play that may lead to increased safety for soccer playing athletes exposed to TBI, the velocity and pressure of soccer balls will be studied closely. Established pressures will be used to simulate in-game kicks that will differ in their velocity. Based on the results, suggestions will surface on how to reduce the risk of TBI whilst maintaining the tradition and nature of the game.

2.2 Theory

2.2.1 Dimensional Analysis

The Buckingham Pi Theorem allows for dimensional analysis of a model through the development of dimensionless and independent groups known as Π-groups. There are a total of $(n_d - k)$ Pi-groups, where n_d is the number of variables of interest and k is the number of base quantities necessary to describe the n_d variables. In this case, the variables of interest are the peak force, F_p velocity, v, pressure, p, diameter, d, and mass, m, of a soccer ball. Having stated the variables, it is important to define them in terms of their base quantity

$$F_p = \left[\frac{ML}{T^2} \right],$$

$$p = \left[\frac{M}{LT^2} \right],$$

$$v = \left[\frac{L}{T} \right],$$

$$d = [L],$$

$$m = [M]$$

where the fundamental dimensions are length, L, mass, M, and time, T. Subsequently, the peak force was identified as the output variable and the remaining four were inputs. Hence,

$$F_p = f(p, v, d, m). \tag{2.1}$$

Due to the fact that $n_d = 5$ and $k = 3$, two Pi-groups have to be formulated.

$$\Pi_o = \frac{F_p}{pd^2}. \tag{2.2}$$

$$\Pi_i = \frac{pd^3}{v^2 m}. \tag{2.3}$$

Given the relationship between the input and output Pi-groups, equation (2.2) can be re-written as

$$\Pi_o = f(\Pi_i). \tag{2.4}$$

Moreover, if the relation between both Pi-groups is assumed to fall under an intermediate asymptotic behavior it can be expressed as $f(\Pi_i) = B\Pi_i^{\beta}$ [37]. The natural logarithm of the Pi-groups is

$$ln(\Pi_o) = ln(B) + \beta ln(\Pi_i), \tag{2.5}$$

an equation that allows to determine the values of the coefficients B and β by recollecting experimental data and utilizing a linear regression. Having identified the coefficients a final expression for the peak impact force was formulated,

$$F_p = (Bpd)\left(\frac{pd^3}{v^2 m}\right)^{\beta}. \tag{2.6}$$

2.2.2 Cotter's Method Sensitivity Analysis

A screening procedure based on a systematic fractional replicate design was developed by Sarah Cotter [38] with the goal of determining the most important factors affecting the result of an experiment. The basis relies on having $2n_p + 2$ trials, with n_p two-level factors. Four scenarios are established; 1) treatment 0, in which all factors are at their lowest level; 2) a total of n trials with treatments ranging from $1, ..., n_p$ where each factors is set at an upper level, whilst the other factors are assigned a low level; 3) treatments $n_p + 1, ..., 2n_p$ for n_p trials where each chosen factor is assigned a low level and all remaining factors are set at an upper level; 4) lastly, a trial where all factors are turned to an upper level.

Having established the trials, an odd and even contrast can be calculated for the effects of the factors, where the factor in turn is denoted by j

$$C_o(j) = \frac{1}{4}[(y_{2n+1} - y_{n+j}) + (y_j - y_0)], \tag{2.7}$$

$$C_e(j) = \frac{1}{4}[(y_{2n+1} - y_{n+j}) - (y_j - y_0)], \tag{2.8}$$

where y is the corresponding output value of the trial. Subsequent, a measure can be estimated, which allows for a categorization of the factors

$$M_{CM}(j) = |C_o(j)| + |C_e(j)|. \tag{2.9}$$

Based on the measure calculated, a sensitivity value, $S(j)$ is quantified by dividing the measure in turn by the sum of all n_p measures.

$$S_{CM}(j) = \frac{M_{CM}(j)}{\sum_{j=1}^{n_p} M_{CM}(j)}. \tag{2.10}$$

In order to rule out levels, the factors in turn are plotted against their respective sensitivity value. Lastly, a screening threshold is put in place corresponding to a value of $\frac{1}{n_p}$. Any sensitivity below the threshold is considered to be not as influential in the experiment.

2.3 Methods

2.3.1 Soccer Ball Parameters

Data recollection was based on the use of six soccer balls with different sizes: two "lightweight" (size 4.5), two size 4s and two size 5s (Figure 2.1). The 4.5 size soccer balls were manufactured by EIR soccer, and known as Global Goals Balls. The aim of these balls being sized as 4.5 is to better adjust for female game play at an elite level, under the argument that size 5 hinder a females ability. The panels making up the EIR ball are machine-stitched thermoplastic polyurethane (TPU) configured in the classic hexagon-pentagon pattern. The size 4 and size 5 used throughout testing were Adidas Starlancer^{TM} training balls, constructed with machine-stitched TPU panels tessellated in a hexagon-pentagon pattern.

One of the variables of interest during testing was the pressure at which the soccer balls were inflated. Thus, two ruling entities in soccer were taken as reference points: 1) at the highest international level, FIFA and 2) at the varsity college level in the United States, the NCAA. According to the 2015-2016 FIFA Laws Of The Game - Law 2, The Ball: Qualities and measurements- the soccer ball should have a pressure equivalent to 8.8 - 16.2 PSI [33]. Similarly, under subsection *2.1 Dimensions* of the NCAA 2016-2017 Soccer Rules and Interpretations the pressure of the soccer ball shall remain between 8.8 - 16 PSI [32]. Taking this under consideration, each ball was tested at four distinct pressures: 4, 8, 12 and 16 PSI. A value below the recommended regulatory boundaries was included to analyze the effect of pressurizing the ball below the manufacturing pressure specifications. The three remaining pressure values were the minimum, maximum and median of the pressure ranges established by NCAA and FIFA. The mass and pressure were measured on each soccer ball before testing, by a scale and a digital pressure gauge respectively.

8

Fig. 2.1. Soccer balls used during testing. The ball sized from left to right are size 4, 4.5 and 5. The size 4 and 5 are Adidas Starlancer™. The size 4.5 is the EIR soccer Global Goals Ball.

2.3.2 Kicking Methodology and Experimental Framework

The experimental framework used to recollect data was comprised of a motion capture system coupled with a force plate. An instep kicking technique was used to launch each soccer ball at the force plate at a distance of approximately 2 meters. Instep kicking was preferred over other types of kicks such as the inside, lofted, outside or curved kick. The reason was due to the fact that a higher velocity can be achieved with an instep kick, whilst maintaining reasonable accuracy [?] [39] [40]. According to Cerrah (2018) an instep kick is described as a kick in which the foot is laterally rotated to an estimated 45 degree angle, whilst engaging the ankle articulation is engaged in plantar-flexion. During impact, the area of contact for the foot is roughly situated where the laces of a shoe are and in regards to the ball, close to its center of mass in the out most layer (Figure 2.2).

Sets of 10 kicks were performed, were the power ranged from low to high for each set. The power behind the kick was monitored by the athlete performing the kicks
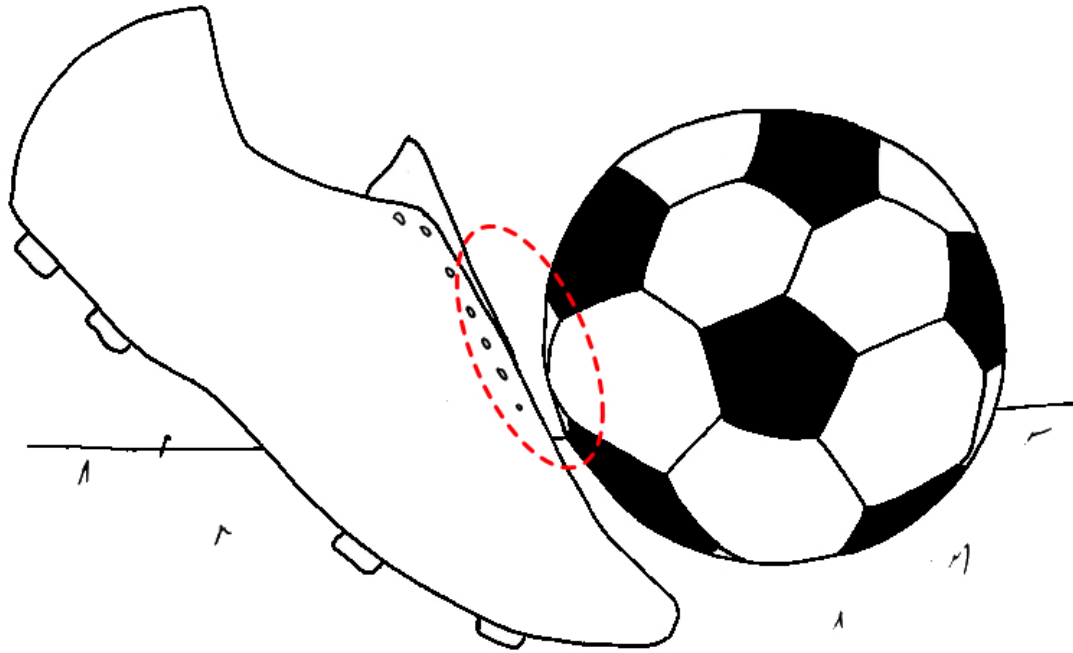
Fig. 2.2. Graphical representation of an instep kick technique. The area of contact between the foot and the ball is delimited by the dotted line. Proper technique should result in the laces of the cleat impacting the ball close to its center of mass.

by means of the force platform. A light tap of the ball was the first kick, followed by the strongest possible impact. After being quantified, these were established as the lower and upper boundaries for that set of kicks. Hence, the remaining eight kicks were kept between this range. Kicks were considered non-standard or unusual if the trajectory of the ball was angled or the impact measured resulted from a rebound or ricochet shot. Unusual impacts were not taken into account and repeated until a clean shot was attained with a perpendicular path. Subsequent to the set of 10 kicks, the pressure was measured with a digital pressure gauge and regulated accordingly

for the following test. In total there were 600 kicks recorded, 200 per ball size and 50 trials per determined pressure and ball size.

2.3.3 Quantification of Force of Impact

A PASCO PASPORT Force Platform® (PASCO, Roseville, CA, USA) was the instrument used to measure the force of the impacts. The force plate provided an area of impact of 35 cm x 35 cm and had a maximum force range of 4400 N. The measurement device was vertically mounted to a back frame with metal beams on either side - to provide stability and reduce the possible noise induced in the data recollection by the vibration motion of the force plate and its subsequent dampening. Special care had to be taken to ensure that the horizontal force being measured was accurate. This included the feet of the plate being in stable contact with the back frame, in addition to the platform being screwed directly to the wooden back frame (Figure 2.3).

Data recollection-wise, the PASCO Force Plate® was limited to a maximum sample rate of 1000 Hz. Nonetheless, when coupled with the PASCO sensor Xplorer GLX (PASCO, Roseville, CA, USA) the sampling rate was increased to a value of 2000 Hz. Sets of testing were initialized by powering up and taring the force platform to zero, making sure resting noise was not part of the output data. Following this, the sensor and force plate were connected to each other through PASPORT® interface. Additionally, both instruments were coupled to a computer that was running PASCO Capstone Software™ as the means to collect the incoming data. Altogether, the PASCO components work in synchrony to allow for accurate data measurements. Through Capstone, a trigger was set in the *"Start/Stop" conditions* at 4 N, which caused a data collection window of 40 ms. The window was made up of two time intervals: a 5 ms post-trigger and a 35 ms pre-trigger. The reason for this was to make sure it encompassed the entirety of the force response wave of each individual impact that was collected. Data was processed through a custom Matlab® script.

Processing consisted of identifying and indexing the peak of each impact response wave, which was later considered to be the peak impact force.
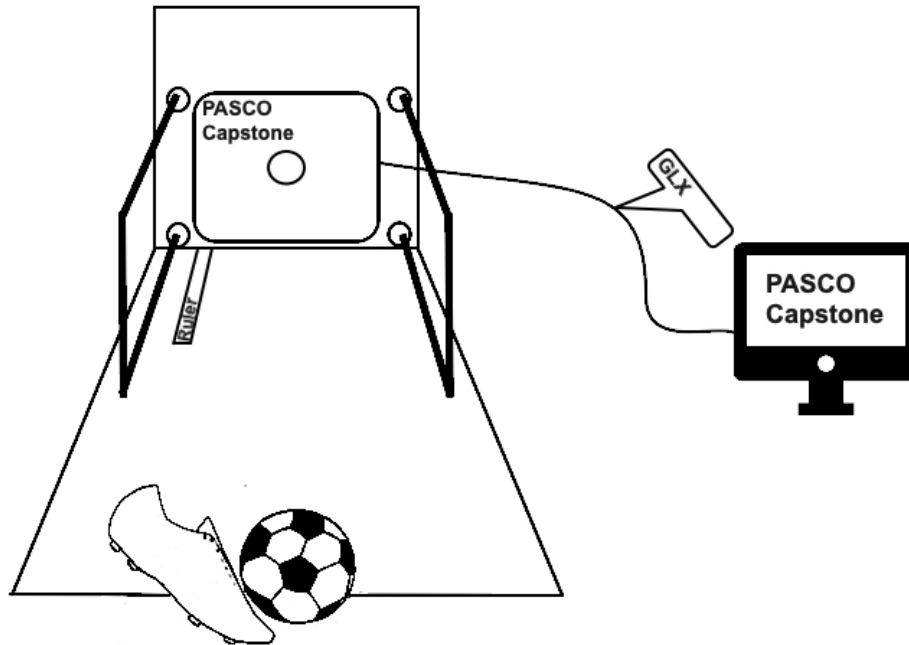
Fig. 2.3. Sketch of the experimental framework used to recollect the data. A force plate was attached to a wooden back-plate that had two supporting arms. The force platform was connected to both the Xlporer GLX and a computer through the PASPORT®interface. An instep kick was performed directly in front of the platform. A ruler was set directly on the balls path, within the cameras frame to help calibrate the distance.

2.3.4   Velocity Data Recollection

In order to measure the velocity, motion capture methods were used. Video recordings were taken of the ball trajectory through a top-mounted camera. Settings on the recording device were adjusted to capture video in a slow motion mode, which did so at 240 frames per second. The recording allowed to view the balls approach to the rig, the deformation of the sphere when in contact with the platform and the final rebound trajectory of the soccer ball after impact.

Measuring tape was aligned to the floor of the rig, making sure it appeared within the video recording. This tool was utilized to calibrate distance measurements in the video clips, through the motion analysis software. Tracker was the video analysis and modeling tool used to process the raw video data. The analysis consisted of tracking the position of the soccer ball frame by frame in the impact video clips. This was done through a combination of manually and automatically tracking an array of pixels in the clips. Regions of interest were chosen on the surface of the soccer ball based on suggestions made by the auto-tracking tool. These included high contrast areas, regions in where there was a change in color or the tracking of specific landmarks on the ball such as a sticker. Having obtained the position and utilizing time data inherent to each frame in the clip, the displacement of the ball was known. Subsequently, the velocity was calculated through analytic derivation of the position data through the video analysis and modelling tool. It is important to note that velocities were measured from both the incoming and outgoing trajectories of the ball. Incoming trajectory was established as the path it took the soccer ball to travel approximately $1.5m$ to the force plate and the deformation stage was evident. The outgoing trajectory began as soon as the ball was no longer in contact with the force platform - or deformed - and the ball was no longer in frame.

2.3.5   Screening Procedure Adapted to Soccer

Based on Cotter's method, the range of values for the factors of interest had to be established. Those parameters pertaining a size 5 soccer ball - mass, diameter and pressure - were isolated according to the FIFA regulations law book. In regards to the velocity values, a literature review was in order that focused on the velocities a soccer ball could experience in different situations prior to heading a soccer ball (Table 2.1). These included throw-ins, long-range passing, crosses, shots and goal kicks. Consequently, the lowest level of the velocity factor was related to a throw-in velocity, whilst the upper level was a consequence of shots on-goal.

Table 2.1.

Upper and lower factor values obtained through literature review for Cotter's Method Sensitivity Analysis

Variable (unit)	Lower Level	Upper Level	Source
Velocity (m/s)	15	30	(Sakamoto et. al, 2013; Koizumi et. al, 2014)
Ball Diameter (m)	0.204	0.221	(NCAA, 2018; FIFA, 2016)
Inflation Pressure (Pa)	58600	111700	(NCAA, 2018; FIFA, 2016)
Ball Mass (kg)	0.397	0.480	(NCAA, 2018; FIFA, 2016)

2.4   Results

2.4.1   Soccer Ball Characterization

The mass and diameter were measured three times at each established ball pressure. The average value for the measurements was calculated (Table 2.2)

The diameter of the EIR soccer Global Goals ball is indeed between the size 4 and 5 Adidas Starlancer[TM]. In terms of the mass, the approximate increase of mass ranged between $11\% - 12\%$ when switching from the size 4 to size 5. The mass of the size 4.5 EIR soccer ball was lower than both other diameter sized balls. More

Table 2.2.

Soccer ball parameters, diameter and mass, categorized by pressure value.

Pressure (Pa)	Mass (kg)	Diameter (m)
Size 4 Ball		
27600	0.387	0.204
55200	0.388	0.205
82700	0.389	0.206
110300	0.391	0.206
Size 4.5 Ball		
27600	0.379	0.213
55200	0.381	0.214
82700	0.382	0.215
110300	0.384	0.215
Size 5 Ball		
27600	0.430	0.211
55200	0.431	0.220
82700	0.433	0.221
110300	0.435	0.221

specifically, there was an increase of 1% and 13% when comparing the 4.5 with the size 4 and 5 respectively.

2.4.2 Impact Force Simulation of a Soccer Ball

The impacts recorded on the force platform were processed within the custom MATLAB script, which allowed to identify the peak impact force, the temporal duration of said impact and an estimate of its impulse (Figure 2.4). Thanks to the recordings a range of data was established for the three descriptors per ball size across all the pressure ranges. The size 4 ball had $201 - 4419N$, and $1.78 - 20.32m/s$ respec-

tively for the peak force and average velocity. In regards to the size 5 $196 - 4667N$ and $1.59 - 20.83m/s$. Lastly, for the EIR 4.5 the ranges were $355 - 4641N$ and $3.33 - 23.37m/s$.
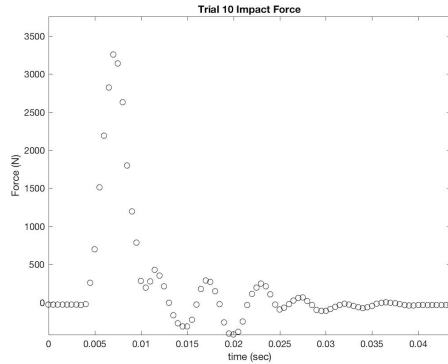
(a) Size 4.
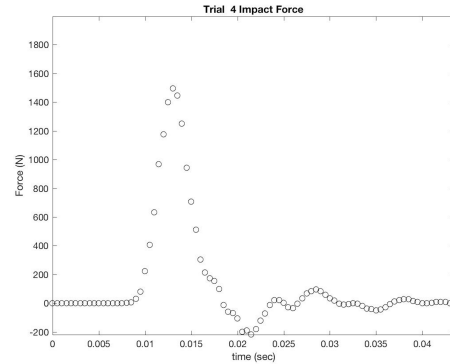
(b) Size 4.5.
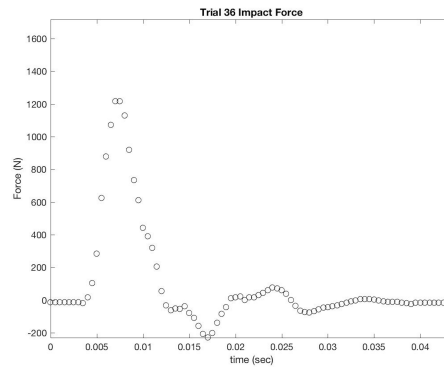
(c) Size 5.

Fig. 2.4. Force wave traces (Force, N, vs time, s) extracted from the PASCO Capstone software. (a) Trial kick for a size 4 ball inflated at 4PSI and travelling at $14.63m/s$. (b) Trial kick for a size 4.5 ball inflated at 8PSI and striking at $17.15m/s$. (c) Trial kick for a size 5 ball inflated at 16PSI with a velocity of $8.13m/s$. Impact duration for the different trials ranged between 0.0045s and 0.017s. A clear peak is evident followed by minor oscillation caused by the vibration of the froce plate post-impact.

Higher incoming velocities result in higher peak impact forces (Table 2.3 and Table 2.4). For both the low and high velocity groups, a trend is noticeable in which by

Table 2.3.

Average peak force in N (± Standard Deviation) for a velocity range classified as high between 14-20 m/s. A tendency is observed where as you increase the ball pressure, the peak force does as well. Alike, by utilizing larger balls, an increase in the peak impact force is expected.

Pressure (Pa)	Size 4	Size 4.5	Size 5
27600	3136 (651)	2580 (377)	2924 (392)
55200	3114 (668)	2976 (431)	3141 (676)
82700	2977 (597)	3078 (412)	3455 (312)
110300	3198 (594)	3328 (474)	3783 (529)

Table 2.4.

Average peak force in N (± Standard Deviation) for a velocity range classified as low between 4-10 m/s.

Pressure (Pa)	Size 4	Size 4.5	Size 5
27600	1113 (430)	987 (302)	1107 (384)
55200	1273 (499)	1257 (353)	1308 (402)
82700	1266 (514)	1323 (422)	1436 (504)
110300	1238 (456)	1403 (465)	1612 (533)

increasing the inflation pressure, the resultant peak force is increased as well. Notably, for low pressures of 4 PSI and 8 PSI the size 4.5 soccer ball has lower average impact forces than the other sizes being tested. Furthermore, for both a low velocity and high velocity range, by decreasing the pressure from 16-8 PSI in a size 5 ball, a 19% and 17% occurs respectively.

2.4.3   Buckingham Pi Theorem

Data recollected from the different trials allowed to demonstrate the linear relationship between the input and output Pi-groups (Figure 2.5). After being plotted, the coefficients were found to be $B = 1.237$ and $\beta = -0.636$, see figure 2.2 and 2.3.

The final form of equation (2.6) was

$$F_p = 1.237(pd) \left(\frac{pd^3}{v^2 m} \right)^{-0.636}. \tag{2.11}$$
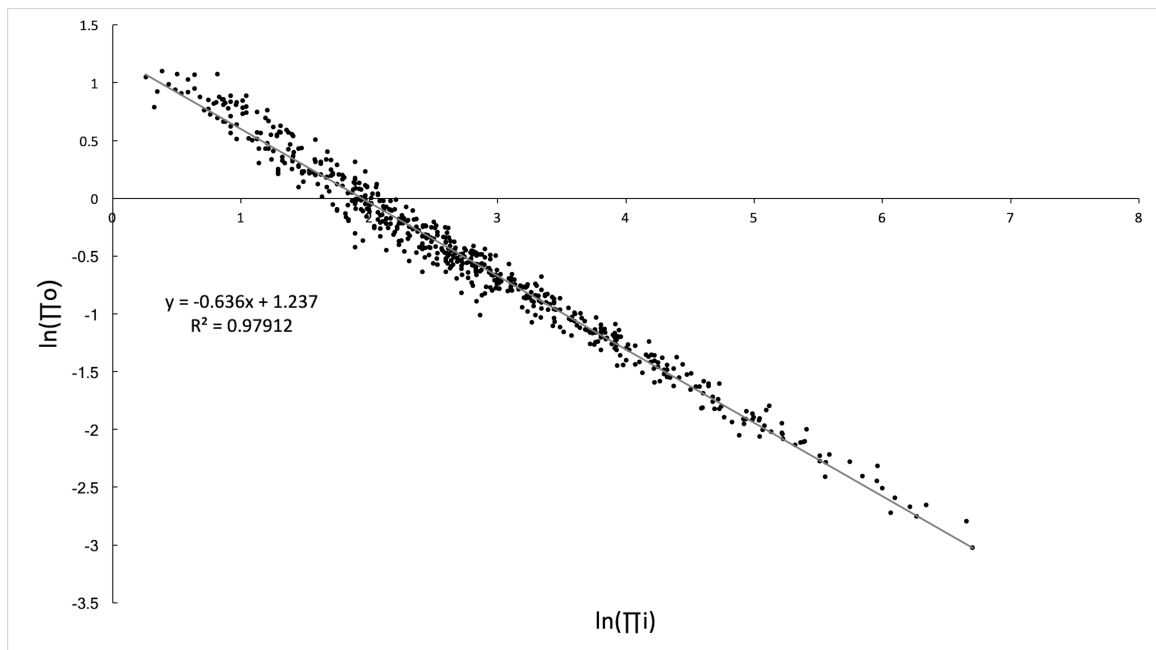
Fig. 2.5. Π_o against Π_i for the entire data set recollected. All ball sizes and pressures are plotted, alongside the linear trendline and its equation. The equation allows to assign values of -0.636 and 1.237 for B and β coefficients respectively. An R^2 value of 0.97 gives insight to the existing linear relationship between in th einput and output Pi-groups.
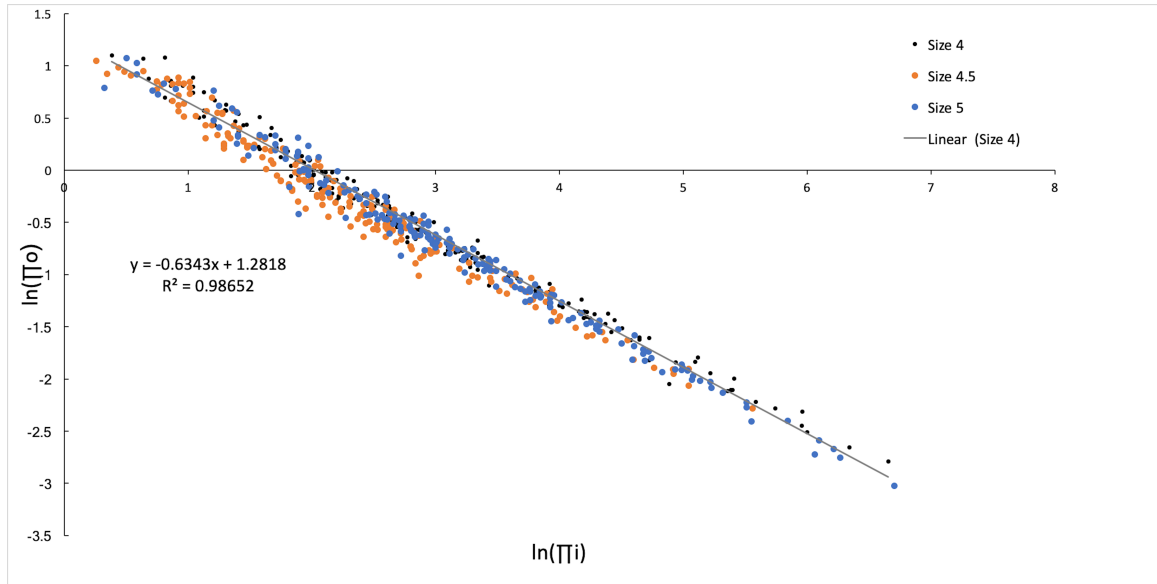
Fig. 2.6. Π_o plotted against Π_i for all the results, but categorized by ball size.

2.4.4 Sensitivity Analysis

According to the analysis made through Cotter's method, a threshold was established with a value of 0.25 equivalent to $1/n_p$, where n_p is the number of factors used. The equation used to calculated the indices was based on the dimensional analysis equation (2.11). The sensitivity index calculated for the velocity was 0.5043, which leads to conclude that it is the factor that affects the peak impact force the most. Second to velocity, was the pressure with an index of 0.4007. The mass and the diameter did not impact the peak impact force as much (Figure 2.7).

2.5 Discussion

Unlike other sports in which contact is intrinsic, soccer players are not required to use protective headgear. Despite recent studies presenting evidence of the brain injuries related to soccer, little to few personal protective equipment is commercially available. Moreover, existent safety equipment are found in the form of headbands,
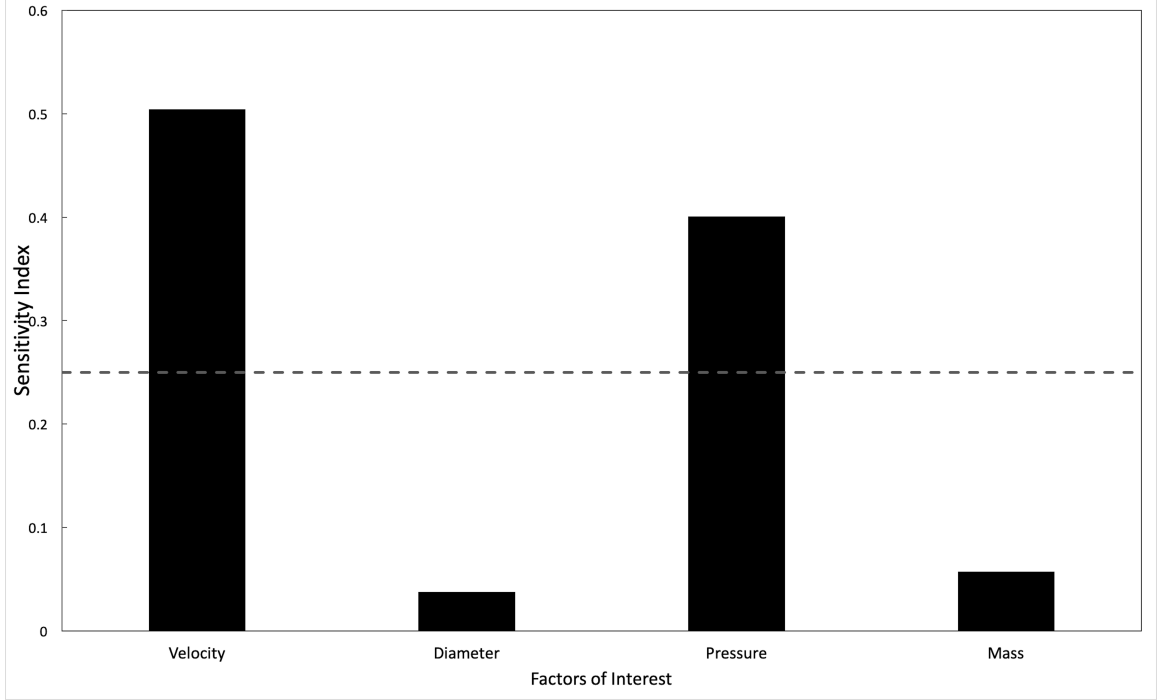
Fig. 2.7. Sensitivity index per factor of interest. The dotted line is equal to $1/n_p = 0.25$, the calculated threshold for influential factors. Both the velocity and pressures sensitivity indices are above said threshold, rendering them more powerful than the other factors.

that have been proven to attenuate impacts within certain ranges [30] [41] but lacked the capacity to mitigate neurocognitive effects of heading [42]. As a means to improved design of headgear in soccer, a proper characterization of the parameters involved during the player-ball collision is required.

According to the sensitivity analysis performed, the variable that most affects the peak impact force during headers is the velocity of the incoming ball, as expected. Nonetheless, due to the nature of the game, controlling the velocity of the ball is not an easy variable to alter. Consequently, the second most influencing parameter, should be the focal point for reducing the risk of TBI due to heading in soccer. The screening procedure prompted this to be the inflation pressure. Based on the data recollected, for velocity ranges typical to a soccer game, changing the pressure from

the upper limit allowed, 16 PSI, to the lower boundary, 8 PSI, can result in a decrease in peak impact force of approximately 20% across the spectrum of ball sizes.

This stated, it would be important to understand how a high impact force could potentially translate to neurocognitive impairment [20]. A measure of the peak linear acceleration (PLA) at the center of mass of the head, alongside the quantification of biomarkers related to neurocognitive symptoms, is a valid approach [6]. Within this study a cohort of 14 athletes were followed during a season of high school soccer. In-game recordings of peak force were taken through worn sensors and coupled with MR imaging to characterize their cerebrovascular reactivity (CVR). Players were subsequently assigned to one of two groups: high load or low load, relative to a measure of cumulative PLA registered for a specific session. The resulting variables of interest can be (Table 2.5), where there is clear evidence that the high load group is receiving a vaster amount of hits at a higher average PLA. In addition, a trend was observed in the study where changes of CVR were seen, when comparing the post-season and in-season session, within the *High Load* group of athletes. No significant changes were seen in the *Low Load* cohort [6]. Thus, it is evident that changes in CVR in these soccer players depended on the cumulative loading of PLA, consequently, being able to shift athletes from high to low loading would result in a mitigation of the risk of neurocognitive impairment.

A manner in which a shift can be achieved is by controlling in-game variables, such as the inflation pressure, ball size and number of hits. Data recollected during this study (Table 2.3) showed that a reduction in pressure from 16 to 8 PSI could result in a 19.7% reduction in PLA, downsizing from a size 5 to 4 would further decrease 7.1% and lastly, a reduction of 20% caused by an arbitrary decrease in the amount of hits, based on the average hit value per player [6]. These factors can translate a *high load* athlete to a *low load* category [43]. Hence, controlling these parameters would ultimately lead to a non-significant change in CVR and a lower risk of neurophysiological alterations.

Table 2.5.

Results from Svaldi et al.'s [6] study showing the session specific variables of interest for both the *High Load* and *Low Load* groups during Post-season. A clear distinction can be seen between both groups, more so, in the rather high average number of hits

	Low Load	High Load
25th Percentile	2425 g	4515
50th Percentile	2930 g	5615
75th Percentile	3800 g	12313
Average No. of Hits	84.1	200.3
Average PLA per Hit	36.3 g	39.5 g

Having identified some of the factors that influence the risk of athletes acquiring TBI, certain modifications can be made to tools used in game or to the rules themselves. With respect to the pressure, a hard-stop pressure regulator can be installed in pumps utilized by soccer players to ensure that the inflation pressure is at a desired and safe value. Law-wise, governing bodies have the capacity of narrowing down the range of allowable pressures by lowering the upper limit. Rigorous enforcement of these inflation values should be followed by part-takers of the sport, no matter the level of play. Leagues and soccer ball manufacturers should also consider utilizing the size 4.5 balls for female athletes. A more venturesome solution would be to aim to lower the amount of headers received by a player during a game. A possibility is to prohibit the header of goal kicks which are known to have high velocities. Players can be reprimanded when doing this, and should only be allowed to use other body parts to receive or control the soccer ball. Referees, coaches and other authoritative figures within soccer should be educated on these issues. Conferences and informative sessions should be held with the aim of teaching these figures how to take preventive measures - whether its pressure, ball size or avoiding unnecessary headers - for their players safe-sake.

Limitations to the study included the dependence on a human to perform the kicks. A level of variability was added, due to no kick being the same. In addition, a high number of kicks were considered unusual, rendering the data useless.

Future studies should focus on quantifying the actual forces experienced by players when heading, in order to custom-fit the factors discussed in this study. In addition, a proper monitoring of elite-level inflation pressure should take place.

3. DESIGN AND MANUFACTURING OF COMPOSITE-BASED PROTECTIVE HEADGEAR FOR SOCCER ATHLETES

3.1 Motivation

Recently, there has been an increased awareness of the risks associated with sustaining short or long term brain damage through participation in soccer [28] [15]. Gessel (2007) demonstrated that soccer is responsible for the highest rate of concussions among female athletes of both high school and collegiate level. Moreover, recent studies have shown that subconcussive impacts have the ability to accumulate over seasons causing neurocognitive and neurophysiological alterations [44] [6]. These changes were observed before, during and after their respective sport season through functional MR imaging [4]. In addition, through the use of transcranial magnetic simulation Di Virgilio et al. (2016) was able to show the acute short term effects heading had on athletes [45]. These studies show that the brains functionality is impaired through the accumulation of subconcussive impacts, suggesting that headgear could be used to mitigate this accumulation.

Reports have indicated that among the different injury mechanisms found for TBI in soccer [27] [46], heading a soccer ball is the most common mechanism of injury [15] [14] [13] [16]. This is voluntary action, where the forehead is used as a multi-purpose instrument in the game. During gameplay, when heading, an athlete at the high school or collegiate level can be exposed to accelerations averaging 40 gs, but possibly exceeding the 100 g mark, from a soccer ball [44] that can reach velocities of approximately 30 meters per second [?] [34]. Recent studies have shown that over 70% of head acceleration events monitored in high school girls soccer are between 20 gs and 40 gs . Furthermore, due to heading not being accidental, it is possible to

simulate and predict the resultant impact forces of a soccer ball travelling at a given velocity [43]. These data allow to understand the mechanics of impacts felt during heading, and consequently, open the possibility for the use of protective headgear.

Unlike other collision sports, there are no existing regulations that enforce the use of protective headgear to prevent subconcussive episodes in soccer. Nonetheless, according to governing bodies, protective headbands are allowed to be used under certain restrictions [33]. However, after simulated testing, several of these headbands have proven to have a poor ability to mitigate severe impacts experienced in-game [30] McIver et al. 2018. A pattern can be identified where headbands are capable of absorbing some energy from high magnitude hits, but not those related to small impacts [17]. That stated, existing protective headgear in soccer does not properly aid in the reduction of a wide range of impact magnitudes felt during game play.

Despite the possible importance of using personal protective equipment during game play in soccer, no existent headgear has the capability of truly diminishing all of the impacts felt in-game caused by heading. Therefore, the goal of this study was to expand on previous research by quantifying the ability of an innovative piece of equipment reduce the physical effects of subconcussive hits in soccer.

3.2 Theory

3.2.1 Dimensional Analysis for Peak Force and Angular Acceleration

Similar to the analysis made in the previous chapter, the Buckingham Pi Theorem was used to model dimensionless Π-groups for the peak angular acceleration and the peak force. This meant that two different input-output relationships would be formulated. The variables of interest, defined in terms of their base quantity are:

$$a_p = \left[\frac{M}{T^2}\right]$$
$$\ddot{\theta}_p = [T^{-2}]$$

$$\int F(t)dt = \left[\frac{ML}{T}\right]$$

$$m_h = [M]$$

$$m_T = [M]$$

$$w_n = [L]$$

$$L_n = [L]$$

$$t^* = [T]$$

where a_p is the peak acceleration; $\ddot{\theta}_p$ is the peak angular acceleration; $\int F(t)dt$ defines the impulse derived; m_h and m_T are the mass of the head and the total mass; L_n and w_n representing the length and the width of the neck; and t^* which is a term that relates the reference time t_r and the time of impact Δt through the equation $t^* = t_r - \Delta t$.

According to the theorem a total of $n_d - k$ Pi-groups must be defined (where $n_d = 7$ and $k = 4$, for both the peak linear acceleration and the peak angular acceleration). Three common input Pi groups were defined

$$\Pi_{i,1} = \frac{(\int F dt)t^*}{m_h w_n} \tag{3.1}$$

$$\Pi_{i,2} = \frac{m_T}{m_h} \tag{3.2}$$

$$\Pi_{i,3} = \frac{L_n}{w_n}. \tag{3.3}$$

In regards to the output variables, $\Pi_{o,1}$ and $\Pi_{o,2}$ correspond to the PLA and PAA terms.

$$\Pi_{o,1} = \frac{a_p(t^*)^2}{w_n} \tag{3.4}$$

$$\Pi_{o,2} = \ddot{\theta}_p(t^*)^2 \tag{3.5}$$

Alike the previous dimensional analysis, an intermediate asymptotic model was used (Barblatt, 2003) to relate the input and ouput Pi-groups

$$\Pi_{o,j} = B_j \Pi_{i,1}^{\beta 1,j} \Pi_{i,1}^{\beta_1,j} \Pi_{i,2}^{\beta_2,j} \Pi_{i,3}^{\beta_3,j} \tag{3.6}$$

where j can either be 1 or 2, depending on the output variable of interest. Hence, applying a natural logarithm to equation (3.6) leads to

$$ln(\Pi_{o,j}) = ln(B_j) + \beta_{1,j} ln(\Pi_{i,1}) + \beta_{2,j}(\Pi_{i,2}) + \beta_{3,j}(\Pi_{i,3}). \tag{3.7}$$

By experimentally obtaining the values for the Pi inputs, it is possible to close down on the solution of the coefficients B_j, $\beta_{1,j}$, $\beta_{2,j}$, $\beta_{3,j}$.

3.3   Methods

3.3.1   Headgear Design

This protective system focuses on the frontal and temporal regions of the skull. Players involved in the game are taught to utilize their forehead as the main area for contact with the soccer ball when heading [46] [47] [31]; . Moreover, there is evidence indicating that the regions that are major sites for head injuries in soccer are both the forehead and temple [48] [49]. Existing commercial protective headgear in soccer focus on the forehead, temple and the occiput [17] [30]. However, the latter is a site that experiences a lower amount of injuries [48], most of these caused through accidental head to head collisions or collisions with the ground [15].

Taking these constraints under account a design of the headband was blueprinted and digitized (Figure 3.1 and 3.2). It is made up of a soft energy absorbing layer and a flexible composite shell. The first, is a 10mm thick silicone padding specifically designed to attenuate a wide range of blows. Silicone padding was encased in a stretchable and breathable fabric to facilitate adhesion to the harder shell. The silicone layer is made up of five smaller pieces, two of which are intended to cover
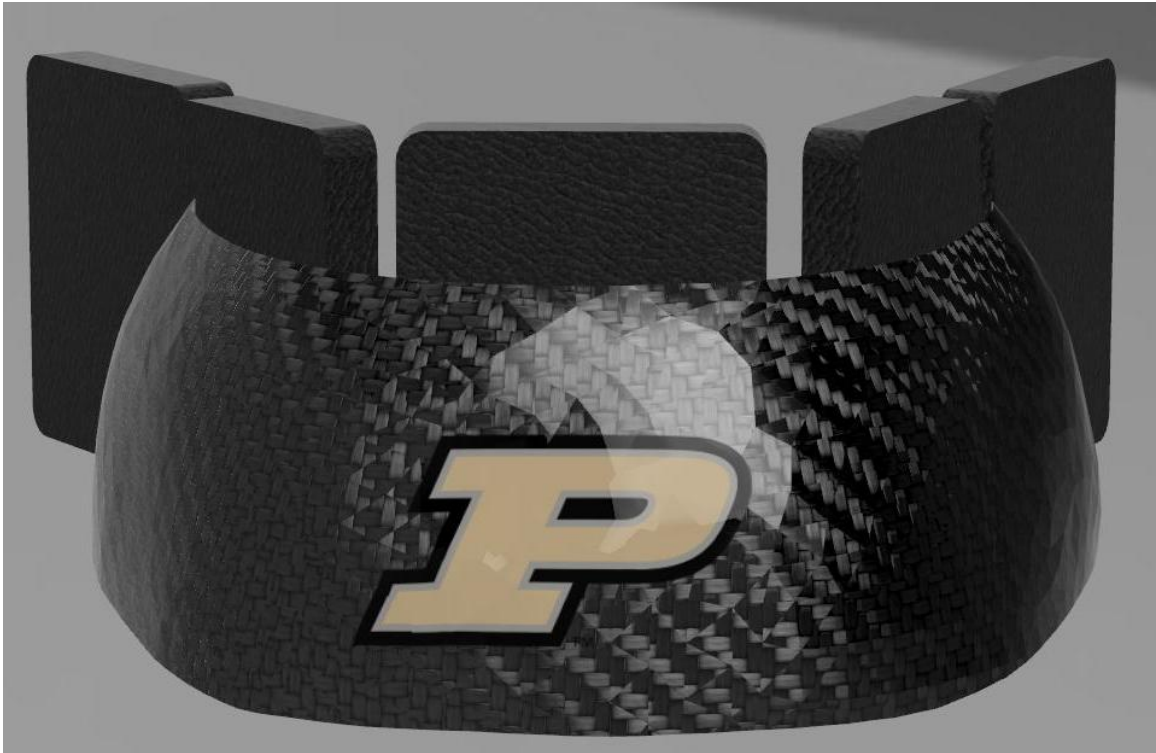
Fig. 3.1. Render of the frontal view of the computer aided design of the headband. Both the composite shell and the padding can be seen.

the front-boss on each side and the remaining part is for the front of the headband. These were attached to the composite shell through fast-acting adhesive. The second layer, is a 6 mm thick composite material plate on the outer-most surface. Epoxy composites are known for their exceptional mechanical properties and highly desirable appearance.

3.3.2   Construction of Tool

In order to manufacture the composite shells, a mold had to be constructed. A three-dimensional scan of a Hybrid III 50th percentile male head (Humanetics Innovative Solutions, Farmington Hills, MI) was performed. The geometry mesh was imported into Fusion 360 (Autodesk, San Rafael, CA), a computer-aided design
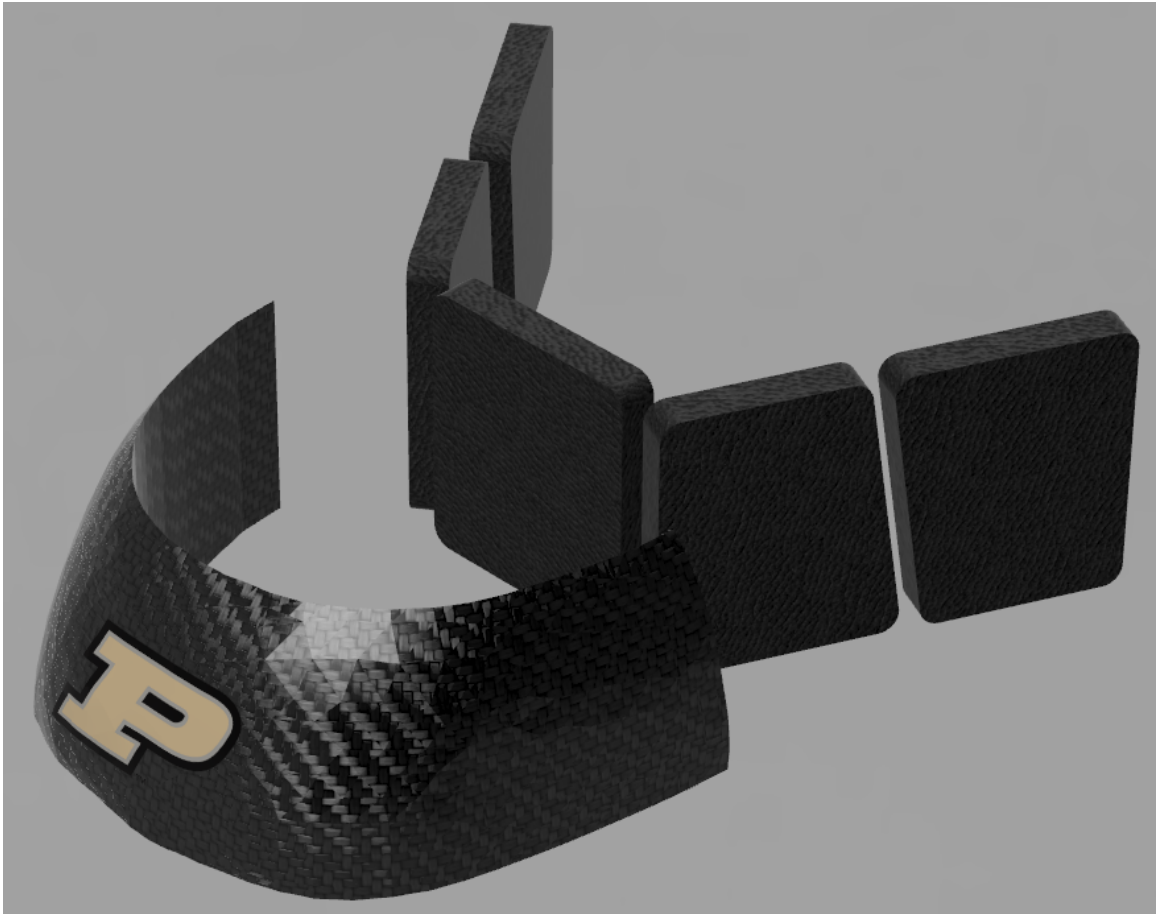
Fig. 3.2. Render of an orthographic view of the computer aided design of the headband. The geometry of the composite shell is visible, as well as the five components of the padding.

software, and converted into a B-rep. By extruding a solid block onto the head geometry, a negative impression of the model was created. Simple commands were utilized to isolate the desired areas: the forehead and temples (Figure 3.3). Further processing was necessary to smooth the surface of interest, which was done through a Laplacian smoothing function in Meshlab [50].

Having obtained the preferred geometry, a computer-aided manufacturing code was generated in MasterCam (CNC Software Inc, Tolland, CT). By means of this code, a computer numeric control machine was utilized to manufacture the mold out

(a) Front View.

(b) Top View.

(c) Orthographic View.
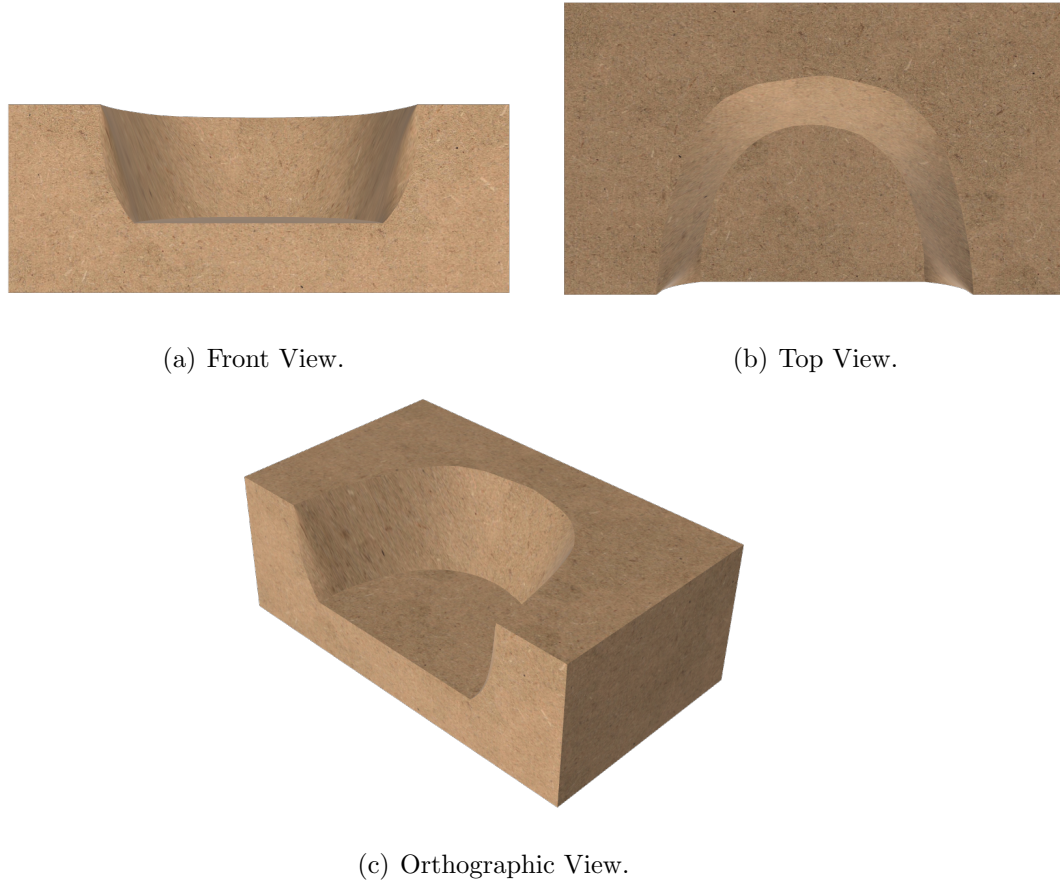
Fig. 3.3. Digital render of the mold designed in Fusion 360. A negative impression of the forehead and frontal bone of the hybrid III head gives the necessary geometry for the composite shell manufacturing.

of wood. Post-processing of the tool included sanding and coating the surface of interest with a coat of epoxy resin (Figure 3.4).

3.3.3 Assembly of Composite Shell

A composite materials was used during the manufacturing of the headbands, which was carbon fiber based. Carbon fiber is widely used material in a variety of industries such as automobile, aircraft and sporting technology [51] due to its mechanical properties, lightweight and moldability [52] [53]. 3K, 2x2 twill weave fabric carbon fiber

Fig. 3.4. Photograph taken of the real tool to be utilized during the manufacturing of the composite shell. MDF was the preferred material during construction, and clear sanding and CNC defects can be seen. A smooth surface finish was obtained, and the shiny appearance is given by the resin coating.

and plain weave Kevlar were the preferred types of fabrics for the manufacturing of the headbands (Fiber Glast, Brookville, OH).

As a means to ensure improved mechanical properties, these fibers are reinforced in a matrix of thermosetting resins. In this case, a chemical reaction-based curing process was used, where epoxide groups within an epoxy resin helped form a complex cross-linked network [54] [51].
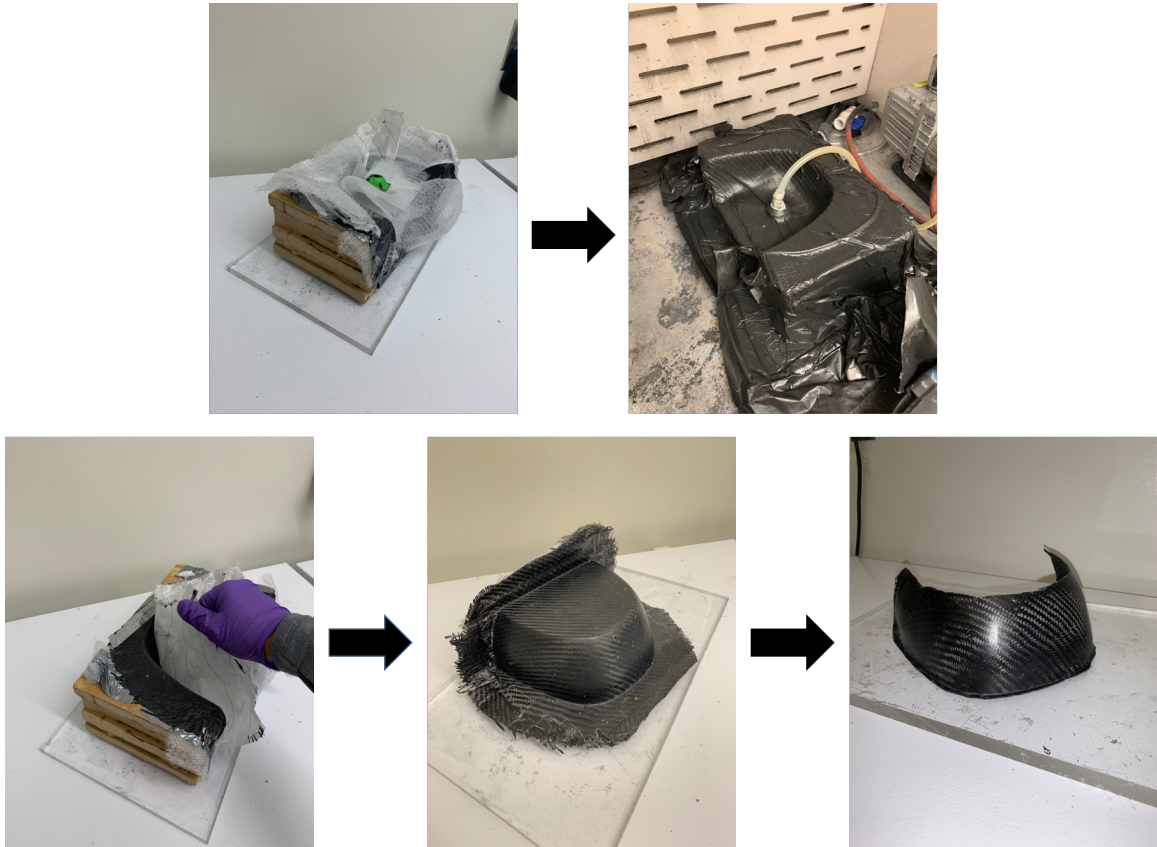
Fig. 3.5. Manufacturing process of the composite shell. The five steps seen include the stacking of the fabrics impregnated with epoxy resin; the use of a vacuum; the initial extraction of the cured carbon fiber piece; total extraction of the part; and the final product after carving the desired geometry

Manufacturing of the product was the same process, no matter the fabric utilized. A vacuum assisted wet layup was favored, due to geometry of the headband mold.

Firstly, strips of 8"x14" of fabric were cut out from 5 yard rolls of textile. The number of pieces being cut out depended on the number of plies being utilized for manufacturing, which was six in this case. Secondly, individual strips were coated in a mixture of IN2 infusion epoxy resin and fast epoxy hardener (Easy Composites, United Kingdom) and carefully placed within the tool. Due to the natural geometry of the head, and consequently the shape of the mold, proper fitting of the strips was complicated. In certain cases relief cuts were necessary, however, these were kept to a minimum as to not introduce stress points within the product. After laying down the required plies, peel ply and breather were stacked on top. Subsequently, a vacuum bag was used to cover the tool and other plies of fabric. A vacuum port was fit in the interface between the bag and the tool, where the vacuum pump was to be connected. Applying a vacuum through the closed molding process allowed for a better surface finish by removing all the entrapped air and speeding the curing process (Park, 2015). It is important to note that the curing process took place at room temperature, which results in a lower glass transition temperature (T_G), desired flexibility and impact resistance. Finally, the piece was removed from the mold and given shape through an oscillating saw (Figure 3.5).

3.3.4   Design and Manufacturing of Padding

The layer of padding included in the headgear is comprised of an in-house manufactured silicone (Eager Polymers, Chicago, IL), unlike other commercially available headbands that utilize layers of foam material. Open cell-foams are typically used in the automotive industry [56], in sport helmets [57] [58] or in military helmets [59]. The typical behavior of open cell-foams during a compression test can has three sections: linear elasticity, plateau and densification (Figure 3.6). In contrast to what is observed with layers of foam, silicone padding is expected to have a unique linear relation between the stress-strain [55]. Through this behavior, the in-house padding
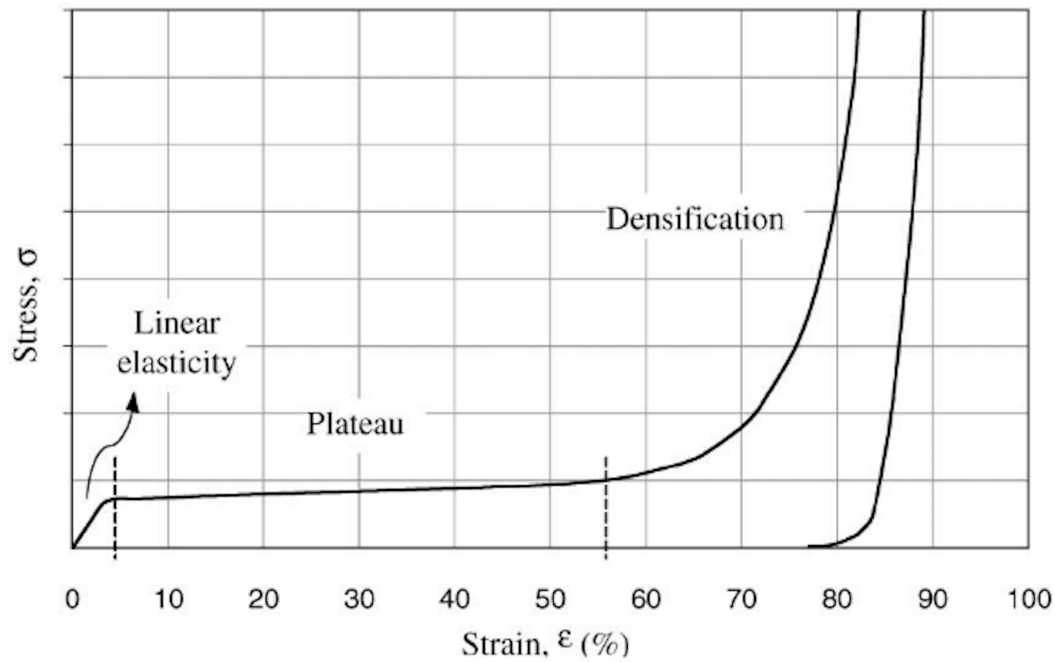
Fig. 3.6. A typical graph of stress versus strain for polyurethane foam
as presented by Avalle et al. (2001) [55]

padding will behave in a more homogeneous manner, no matter what load is being
applied, thanks to its degrees of porosity.

Manufacturing of the padding was split in different steps. Firstly, a 3D printed
mold had to be designed in Fusion 360. The tool included two types of portrusions,
a cylinder and half a sphere, for desired features of the first degree of porosity. At a
superficial level, these portursions would result in hollow indentations within the block
of silicone. Subsequent to the printing of the mold, the silicone had to be prepared to
be poured. One of the constituents of the RTV 1000 (Eager Polymers, Chicago, IL)
mixture were graphite particles. These particles added the second degree of porosity
at a millimeter level scale. Lastly, the four hour curing process of the silicone inside
the mold took place within a vacuum bell. By releasing entrapped air in the mixture,
a third degree of porosity at a micro level was obtained (Figure 3.7).
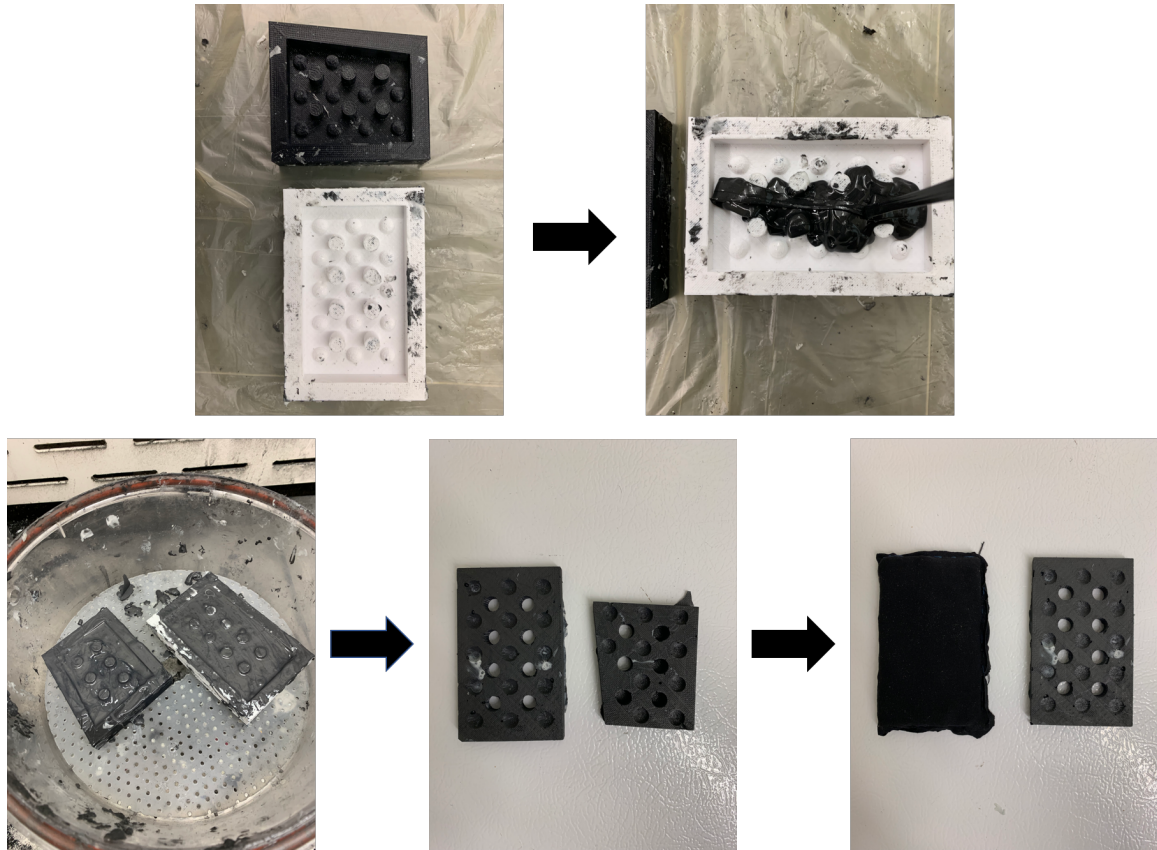
Fig. 3.7. Manufacturing process of the padding pieces. The first image shows the 3D printed molds which include the cylinders and half spheres that allow for a degree of porosity. Second, an image where the pouring of the polymer within the molds can be seen. In third place, the molds and polymer are placed within a vacuum bell. Fourth, the cured product is removed from the bell and the post-vacuum pieces are extracted from the molds. Lastly, the manufactured silicone is encased in a breathable, stretchable fabric.

3.3.5 Experimental Testing of Protective Headgear

The experiment was designed to simulate the impacts delivered in practices and games during head injury related mechanisms. Manufactured protective equipment was fitted on a Hybrid III 50th percentile male head and neck that was fixed on a 80 kg steel block. The hollow space within the head is filled with an array of accelerometers

arranged in a 3-2-2-2 setup [60]. These measuring instruments generate an estimated value of acceleration at the center of mass of the head, which is then passed to a National Instruments model 9234 DAQ module (National Instruments, Austin, TX). Similar to the accelerometers, a model 086D20 impulse hammer (PCB Piezotronics Inc, Depew, NY) was coupled with the DAQ systems, as the tool used to record the impulse and force values of the simulated impacts.

The DAQ acquisition module was utilized to digitize the hammer and accelerometer voltages by means of a custom software functioning at a sampling frequency of 5120 Hz. Raw incoming signals were processed through custom Matlab Code [60] that could output peak translational acceleration (PTA) and peak angular acceleration (PAA) at the center of mass of the Hybrid III head. In order to do so, kinematic equations describing the impacts were solved. By obtaining data recordings of the PTA and PAA, it was possible to use them as inputs in the dimensional analysis.

Twenty impacts were dealt to the locations of interest of the headband. Four sets of five strikes were recorded at the following approximate g-force acceleration ranges: <20g, $21-40$g, $41-60$g, $61-80$g and $81-100$g. The designated locations of interest for impact testing were front, front-boss and side (Figure 3.8). It is important to clarify that only the right side was impacted, a symmetrical response to impacts was assumed for both the right and left side. Each location was struck by the hammer normal to the surface and at a 45° angle. A total of 120 hits were registered per headband. The composite material based headbands were compared with three different commercial headbands. These included the Storelli Exoshield Head Guard, the Full 90 and the Second Skull.

3.3.6 Statistical Analysis for Impact Attenuation

Based on the dimensional analysis performed, it was possible to obtain values for the B and β coefficients through a simple linear regression. As a means to remove outliers, a modified version of Grubbs' method was implemented. A value for a
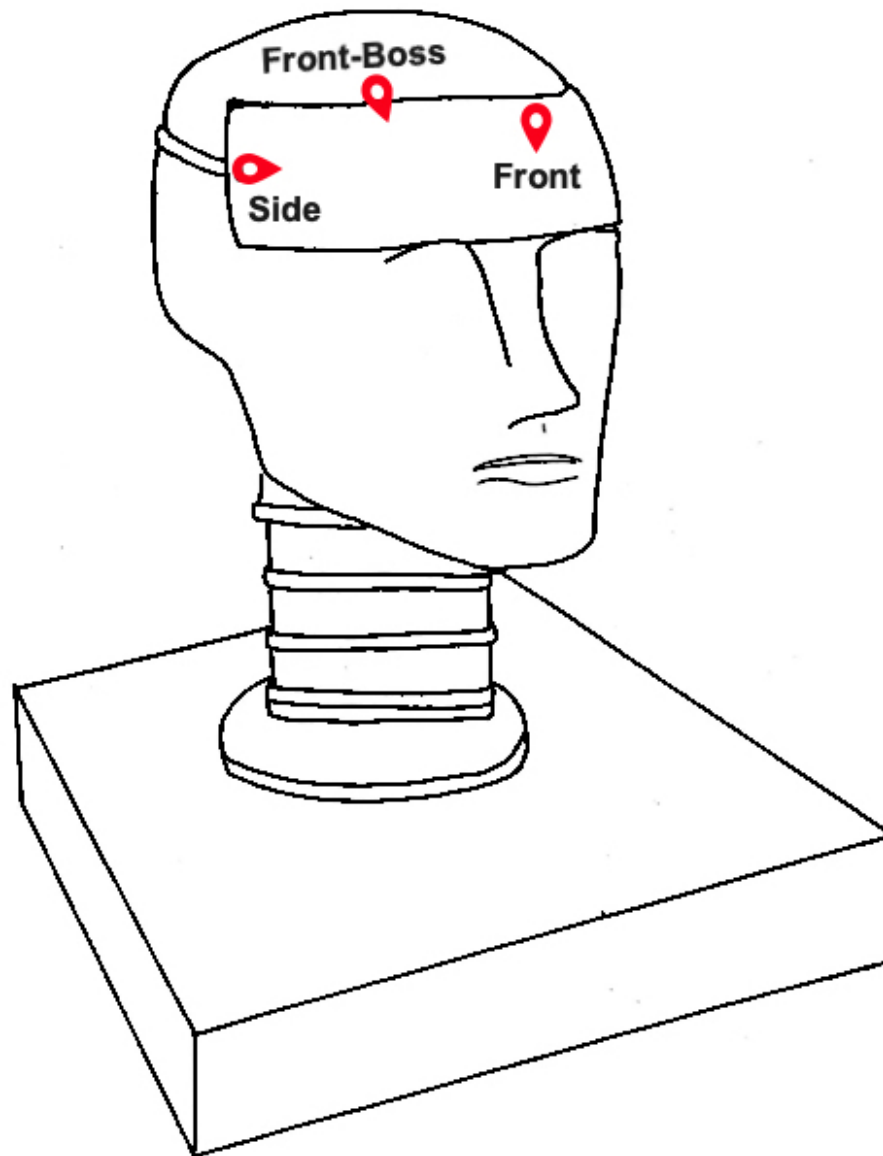
Fig. 3.8. Digitized sketch of the experimental setup. A 50th percentile Hybrid III male head was used for testing. The composite material headband was placed across the frontal and temporal areas of the head form. A modal impulse hammer was used to strike the protective equipment on the three sites highlighted in red: the front, front-boss and side.

standard deviation between the original data set and data curve fitted to the simple linear regression was calculated. Data points were removed from the data set if they were more than three standard deviations from the curve fitted data. A final

curve fit was performed to the new data set, to calculate values for the B and β coefficients. Following this, an analysis of covariance (ANCOVA) was utilized to evaluate the coefficients obtained from the unhelmeted Hybrid III head and each headband tested [60].

In addition, an effect size was quantified to further the comparison between existing head gear and the in-house manufactured headband. A minimum and maximum impulse were identified for the data set being analyzed per headband and location. 100 more impulse values were chosen, evaluated and averaged per location for the established range. This statistical measure gives insight on the average difference between groups in regards to to the overall variability [60].

3.4   Results

3.4.1   Headband Manufacturing

The construction of the protective headgear was successful for the most part. Five sets of padding were built to specification and easily adhered to the composite shell. The dimensions and geometry allowed for proper fixation to the outer shell as well as tight fitting on the hybrid III head. Padding stayed encased within the stretchable, breathable fabric and did not suffer major damage during testing.

In regards to the composite shell, a total of 6 headbands were manufactured: three 3-ply thick and three 6-ply thick headbands. The vacuum assisted wet layup allowed impregnation of a vast majority of the composite shell, however, the epoxy resin did not permeate the entirety of the fabric. This resulted in a series of dry spots where mechanical failure can occur with ease. In spite of the headbands being extracted out of the mold successfully, after an initial round of testing, delamination occurred vertically around the mid-line of the headband due to mechanical load (Figure 3.9).
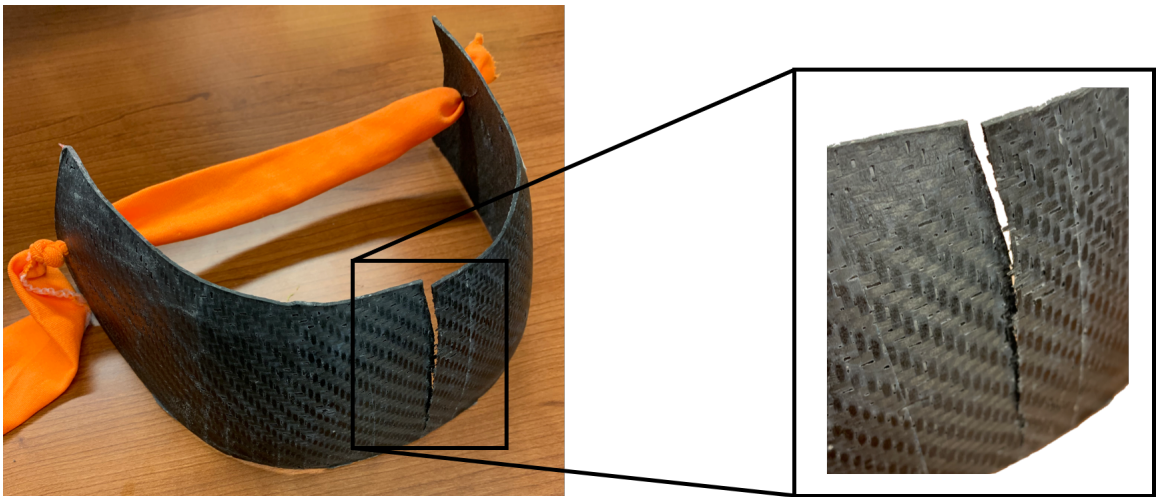
Fig. 3.9. Sample of headband after testing. Delamination is evident across the vertical mid-line of the product.

3.4.2   Dimensional Analysis and Impact Analysis Testing

After performing the data recollection, it was clear that the input Pi-group of interest was only $\Pi_{i,1}$. Due to the fact that the mass of the Hybrid III head was constant, the value of m_T would slightly vary from helmet to helmet. Nonetheless, the overall value of $\Pi_{i,2}$ did not fluctuate in a consequential manner. In regards to $\Pi_{i,3}$, the Hybrid III neck was not changed during testing. Thus, the calculated value of the dimensionless group would vary at all. This stated equation 3.7 was simplified to

$$ln(\Pi_{o,j}) = ln(B_j) + \beta_{1,j}ln(\Pi_{i,1}). \tag{3.8}$$

Therefore, a simple linear regression would yield the values of the coefficients in both scenarios.

The ANCOVA results (Table 3.1) indicate that the in-house composite material based headgear manufactured did not perform well (highest value of β_{11}). However, for the location tested, all of the estimated β_{11} were above unity. In other words, within this location the headgear tested does not do the best job to mitigate the impacts as the dimensionless impulse increases.

By plotting the $\Pi_{o,1}$ and $\Pi_{o,2}$ against $\Pi_{i,1}$ (Figure 3.10) the overall performance can be evaluated. When analyzing the peak translational acceleration, the 6 layer manufactured helmet (labeled IOC6) performs best at low impulse values. It tends to the other headgear at higher $\Pi_{i,1}$ values. Interestingly, across the entire impulse spectrum all the commercially available helmets have a behaviour similar to the unhelmeted hybrid III headform. The effect size calculated for the translational acceleration (Table 3.X) indicates that the CF 6-Layer has a substantial effect when compared to an unhelmeted headform (value above unity).

In regards to the angular acceleration ($\Pi_{o,2}$), none of the headbands tested has an effect (Figure 3.10). The data points recollected are clustered around the trend-line
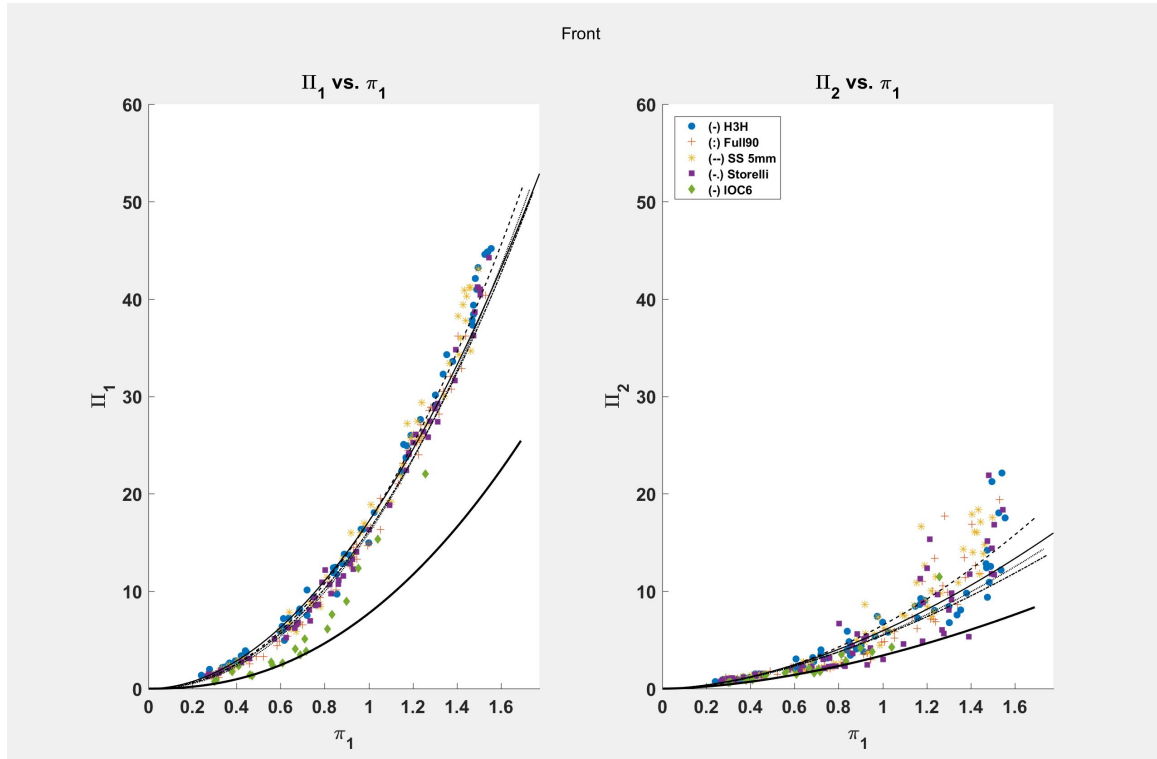
Fig. 3.10. $\Pi_{o,1}$ (left plot) and $\Pi_{o,2}$ (right plot) versus $\Pi_{i,1}$ for an unhelmeted Hybrid III head form and the headgear tested - Full 90, Second Skull, Storelli Exoguard and CF 6-Layer.

Table 3.1.
ANCOVA statistical results for the dimensionless groups $\Pi_{o,1}$ and $\Pi_{o,2}$, between types of headgear denoted with letters. The annotations a, b, c and d indicate significant difference between the unhelmeted Hybrid III headform, Full 90, 2nd Skull, Sotrelli Exoshield and the CF-6 Layer prototype respectively.

	Front Location		
	Coefficient	$\Pi_{o,1}$	$\Pi_{o,2}$
Hybrid III	B_1	17.54 (bcde)	6.05
	β_{11}	1.96 (bcde)	1.73
Full 90	B_1	15.96 (acde)	5.54
	β_{11}	2.13 (ad)	1.73
2nd Skull 5mm	B_1	17.17 (abde)	6.51
	β_{11}	2.07 (ae)	1.89
Storelli ExoShield	B_1	16.24 (abce)	5.46
	β_{11}	2.05 (abe)	1.65
CF 6-Layer	B_1	10.81 (abcd)	4.38
	β_{11}	2.27 (acd)	1.71

of the unnhelmeted headform. None of the effect sizes (Table 3.2) are above unity, moreover, the commercially available headgear are closest to 0.

Table 3.2.
Effect size compared from each headband to the unhelmeted Hybrid III headform. An effect size greater than unity is desired.

Parameter	Full 90	Second Skull	Storelli	CF 6-Layer
$\Pi_{o,1}$	0.8	0.21	0.6	2.45
$\Pi_{o,2}$	0.18	0.21	0.2	0.54

3.5   Discussion

During the fabrication of the headbands, the fabric strips of carbon fibers used to construct the composite shell were not uniformly impregnated with epoxy resin. A wet layup does not ensure that the distribution of the thermoset resin is homogeneous across all the plies being used after the curing process. These are known as macro voids - or dry spots - and are considered manufacturing defects caused by an irregular flow front of the resin [61]. In spite of the flow front being guided by the use of a vacuum, the rate of suction in combination with the cyring time of the epoxy was not completely accounted for. As a result of epoxy resin not impregnating all the layers of fabric, the interlaminar bonding is weak and can cause a mode of delamination known as tearing due to shear [62]. A mode in which this could have happened was that the plies tore apart from each other in response to the impacts being dealt by the hammer.

Another possibility, is the response the shell had to the experimental testing setup. The headband was placed on the forehead of the Hybrid III head and kept secured through an elastic band tied to the ends of each side. In an attempt to maintain the product firmly mounted on the head, the elastic band was thoroughly tightened. As a consequence, a three point bending scenario was established. Each fixture point of the elastic band acted as a supporting pin and the strike on the forehead from the impulse modal hammer would apply the load to the composite shell. A three-point laminar flexure test induces shear in the lamina of the specimen, leading to a tearing delamination failure mode [62].

Different materials should be explored for the manufacturing of the headbands. Kevlar, an aramid fiber, could be a substitute, known for its flexibility, durability and its characteristic strength which exceeds steels' by five-fold [63]. These and other mechanical properties [64] make the material attractive for a variety of applications including tactical bullet-proof vests and airplane components [65]. The use of 6 kevlar plies is not necessary though, carbon fiber plies can be used interchangeably.

That stated, the headbands manufactured with carbon fiber showed potential. At low impulse values, the performance seen for the peak linear acceleration was better in comparison to the other commercially available helmets. The addition of a hard outer layer to the padding improves the performance. The lone composite shell allows for the distribution of the force across a larger surface. The statistical analysis rendered the same conclusion, an effect size above unity and a low $\beta_{1,1}$ indicate the superior performance. However, when analyzing the angular acceleration, the performance was not as great. Despite the effect size being larger than the other headbands, it was not above unity. Hence, there was no marginal difference between the use of the 6-layer carbon fiber headband and not using protective equipment. However, a reduction in PAA is not expected in headgear that is firmly affixed to a head and does not expand out.

4. FREQUENCY DOMAIN EVALUATION OF IMPULSE ATTENUATION BY FOOTBALL HELMETS

4.1 Motivation

Protective head gear is a requirement in a variety of sports in which athletes are constantly involved TBI related incidents. Some of these sports include American football [18], hockey [66], lacrosse [67](and boxing [3]. According to Levy (2004) [68] the use of helmets has been obligatory in American football for more than 70 years. Leather helmets that lacked chinstraps and even face-masks evolved over the years to a version that fulfills the needs of the modern game. Nowadays, helmets have chinstraps, steel face-masks and a plastic-shell lined up with padding or some other cushioning instrument comprised of air-bladders, polyurethane foams or other liner systems [69]. Performance of protective head gear can be evaluated through different standards developed to quantify the capability the gear has to protect its user against brain injury [70]. Standards can be contributed to organizations such as ASTM International and NOCSAE. ASTM International elaborated an American national standard, ASTM F717-10, focused on shock absorption capabilities and requirements for materials and manufacturing through impact testing [71]. Nonetheless, it was withdrawn in 2017 "due to its lack of use in Industry" [71]. In contrast, the standard written by NOCSAE (2007) is widely used in the industry as a certification program characterized by its use of the Gadd Severity Index [72].

Compliance with these standards and the need to certify helmets for commercial use, has driven the design of helmets to focus on the prevention of skull fractures and/or other major head trauma. Notwithstanding, recent evidence has been presented by various studies highlighting the fact that repetitive impacts to the head can lead to alterations in an athletes neurophysiological [8] and neurocognitive [5]

development. These kind of head acceleration events do not necessarily result in skull fractures and thus, are overlooked by the NOCSAE grading system [5] [73] [20]. For this reason, other design parameters should be taken into account that may possibly encompass brain injuries that range across the entire spectrum of head acceleration events. Two of these new parameters include the transmissibility and mechanical impedance of helmets used in American football. These variables can be quantified to evaluate the energy absorption of materials through a range of impact loads.

Therefore, a study was performed to understand how the use of frequency domain variables is instrumental to evaluate the performance of protective head gear in contact sports. Simulated and in-game impacts were utilized to determine a frequency range of interest with biomechanical relevance. The resulting Frequency Range of Interest (FROI) was used to help characterize the transmissibility and mechanical impedance of two helmets.

4.2 Theory

4.2.1 Transmissibility

In vibration mechanics, the ratio of output to input accelerations as a function of frequency can be defined as the transmissibility [74] [75] [76].

$$T_{HD,HT} = \frac{\ddot{X}_{HD}(\omega)}{\ddot{X}_{HT}(\omega)} \tag{4.1}$$

where $\ddot{X}_{HD}$ and $\ddot{X}_{HT}$ represent the acceleration experienced by the head and helmet in the frequency domain, respectively.

4.2.2 Mechanical Impedance

By measuring the output at a point A on the head, $\ddot{X}(\omega)$, and transforming the input force in the time domain, $f_B(t)$, to the frequency domain, $F_B\omega$ the frequency response function, $H_{A,B}(\omega)$ is defined theoretically as

$$H_{A,B} = \frac{\ddot{X}_A(\omega)}{F_B(\omega)}, \tag{4.2}$$

where $\ddot{X}_A(\omega)$ corresponds to the acceleration output in the frequency domain measured at point A (Figure 4.1). Furthermore, the acceleration frequency response function (FRF) is associated to the displacement FRF by a factor of $-\omega^2$ (a more detailed derivation can be found in the following subsection). Thus, equation (4.2) can be rewritten as

$$H_{A,B} = -\omega^2 \frac{X_A(\omega)}{F_B(\omega)}. \tag{4.3}$$

where $X_A(\omega)$ is a frequency domain representation of point A.

On the basis of equation (4.3) the displacement experienced by the head and helmet (Figure 4.2.c) is formulated as

$$X_{HD} = -\frac{-1}{\omega^2} H_{HD,HD} F_{HD}. \tag{4.4}$$

By considering that there are external forces being applied on the helmet by both the external stimuli and the head pushing up against it, an equation for the displacement transmitted to the head is derived,

$$X_{HT} = -\frac{-1}{\omega^2} (H_{HT,HT} F_{HT} - H_{HT,HD} F_{HD}). \tag{4.5}$$

Due to an existing interaction between the padding of the helmet and the force being experienced on the head, F_{HD}, the spring constant, k_{HT}, and damping coefficient, c_{HT}, have to be considered as constraints (Figure 4.2.b).

$$f_{HD} = k_{HT}(x_{HT} - x_{HD}) + c_{HT}(\dot{x}_{HT} - \dot{x}_{HD}). \tag{4.6}$$

After transferring the equation to the frequency domain, and considering an expression for the coupling force between a head and a helmet, $Z(\omega)$, the force can be described as
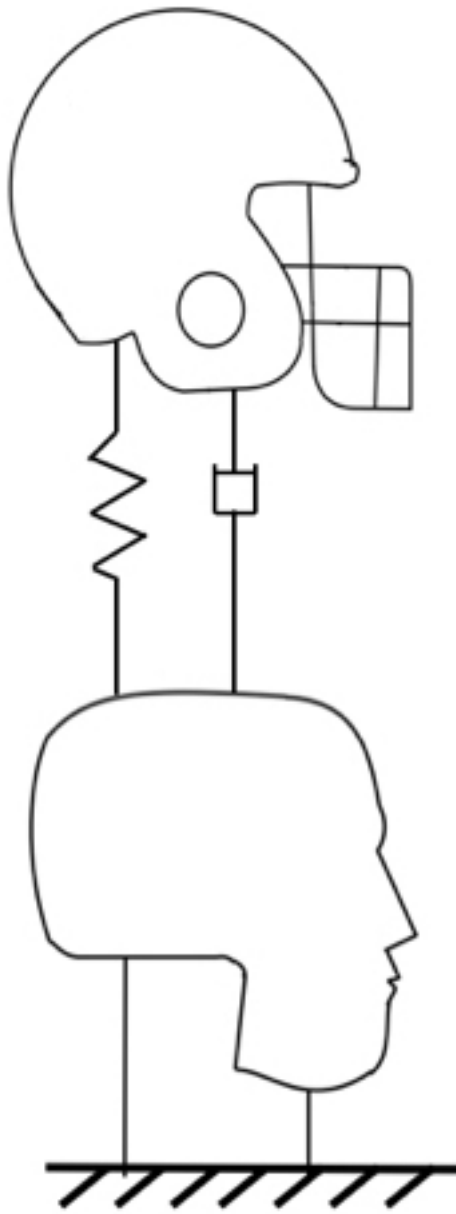
Fig. 4.1. Diagram demonstrating the basic mechanical impedance model, in which there are two point of interest A and B. Force is being applied at point B and acceleration is measured at point A. Through this interpretation it is possible to relate input force and output acceleration to formulate a frequency response function $H_{A,B}(\omega)$.

$$F_{HD}(\omega) = Z(\omega)(X_{HT} - X_{HD}). \tag{4.7}$$

It is important to note that the padding can be modeled by a dynamic impedance formulated as $Z(\omega) = k + \omega ic$. Having described the coupling relationship between the forces experienced by the head and helmet, the FRF for the force measured at a point on the helmet and the output acceleration measured within the head, $H_{HD,HT}(\omega)$ can be computed theoretically by substituting eq. (4.7) into both equations (4.4) and (4.5),

$$H_{HD,HT}(\omega) = \frac{H_{HT,HT}H_{HD,HD}Z(\omega)}{(-\omega^2 H_{HD,HD})Z(\omega) - \omega^2}. \tag{4.8}$$

The value for $H_{HD,HT}(\omega)$ can be quantified experimentally, thus, allowing to solve equation (4.8) for the variable of interest: $Z(\omega)$

$$Z(\omega) = \frac{-\omega^2 H_{HD,HT}}{(H_{HT,HT}H_{HD,HD}) + H_{HD,HT}(-\omega^2 H_{HD,HD} - H_{HD,HT})}, \tag{4.9}$$

where ω^2 and the remaining FRF's can be identified through experimentation.

Frequency Domain Relationship between Displacement and Acceleration

A valid assumption that can be made is that the padding lining a helmet can be treated as single-degree of freedom system.

The sum of the vertical forces can be formulated as

$$\sum \vec{F} = m\vec{a} = m\ddot{x} \tag{4.10}$$

$$m\ddot{x} = -c\dot{x} - kx + F(t), \tag{4.11}$$

where F, is the force being applied to the system; m, is the mass; c is the damping ratio; k, is the stiffness; $\ddot{x}$ is the acceleration; $\dot{x}$ is the velocity and x is the displacement experienced by the body. By rearranging equation (4.11)
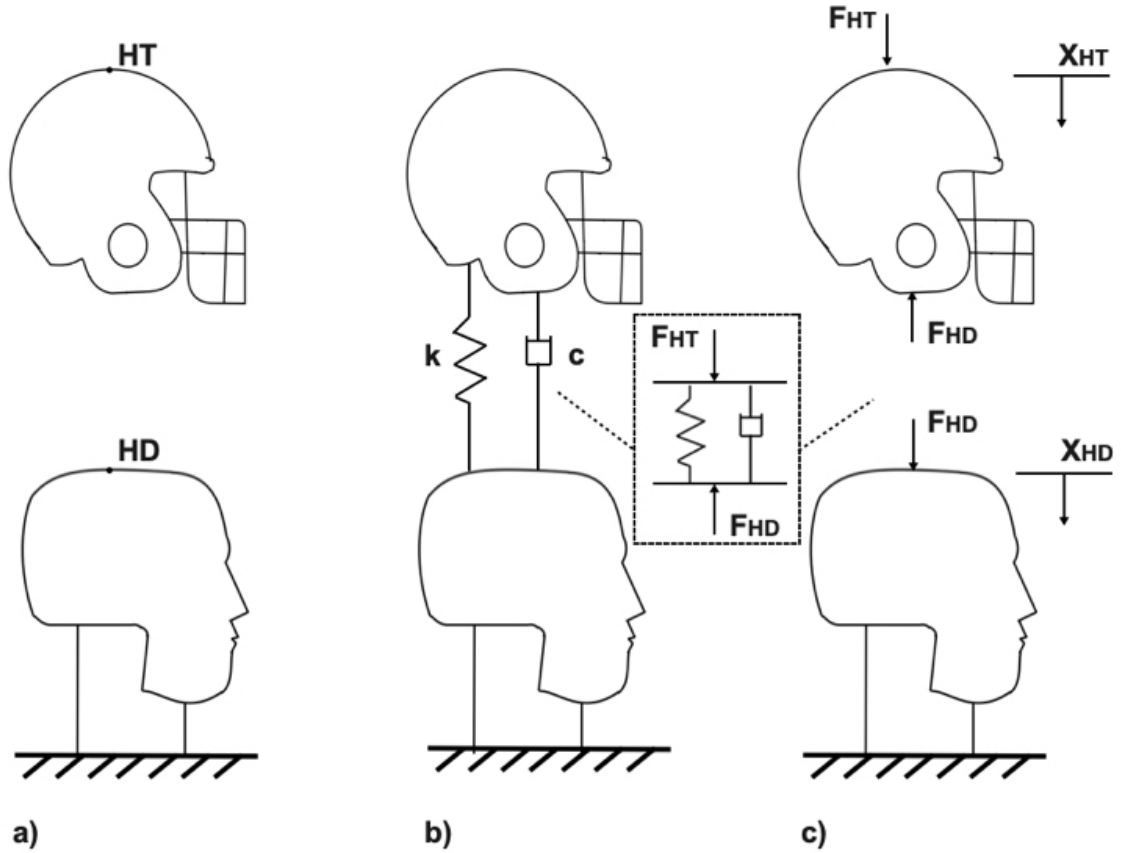
Fig. 4.2. Visual representation of the experimental setup. a) Point of interest where measurements were taken for the hits dealt on the Hybrid III head, or helmet; b) padding modeled as a spring-dashpot system, used to model the impedance of the system; c) body diagram of the forces and displacement experienced by the Hybrid III head and helmet during impact.

$$\frac{1}{m}F(t) = \ddot{x} + \left(\frac{c}{m}\right)\dot{x} + \left(\frac{k}{m}\right)x \qquad (4.12)$$

The natural angular frequency of a free damping mass and spring system can be expressed as

$$\omega_n^2 = \frac{k}{m}.$$

Similarly, an expression can be formulated for the damping ratio and angular frequency

$$2\xi\omega_n^2 = \frac{c}{m}.$$

In addition, the force being applied to the system can be described through the following function

$$F(t) = F_0 sin(\omega t).$$

By substituting these conventions into equation (4.12)

$$\frac{\omega_n^2}{k}F_0 sin(\omega t) = \ddot{x} + 2\xi\omega_n^2\dot{x} + \omega_n^2 x, \tag{4.13}$$

the previous governing equation can be solved through a Fourier transform, thus,

$$\int_{-\infty}^{\infty}\left[\frac{\omega_n^2}{k}F_0 sin(\omega t)\right]e^{-i\omega t}dt = \int_{-\infty}^{\infty}[\ddot{x} + 2\xi\omega_n^2\dot{x} + \omega_n^2 x]e^{-i\omega t}dt. \tag{4.14}$$

In order to solve this equation, the integral on the right hand side will be separated into three integrals

$$\int_{-\infty}^{\infty}\left[\frac{\omega_n^2}{k}F_0 sin(\omega t)\right]e^{-i\omega t}dt = \int_{-\infty}^{\infty}\ddot{x}e^{-i\omega t}dt + \int_{-\infty}^{\infty}2\xi\omega_n^2\dot{x}e^{-i\omega t}dt + \int_{-\infty}^{\infty}\omega_n^2 xe^{-i\omega t}dt$$
$$\tag{4.15}$$

The individual integrals will be solved from here on. The first integral concerns the displacement term

$$\int_{-\infty}^{\infty}\omega_n^2 xe^{-i\omega t}dt = \omega_n^2\int_{-\infty}^{\infty}xe^{-i\omega t} = \omega_n^2 X(\omega). \tag{4.16}$$

Where the displacement function in the frequency domain is defined as

$$X(\omega) = \int_{-\infty}^{\infty}xe^{-i\omega t}dt. \tag{4.17}$$

Secondly, the integral that includes the velocity term can be solved by parts

$$2\xi\omega_n^2\int_{\infty}^{\infty}\dot{x}e^{-i\omega t}dt = 2\xi\omega_n^2\left[x(t)\Big|_{\infty}^{\infty} + (i\omega)\int_{\infty}^{\infty}xe^{-i\omega t}dt\right].$$

As the term t approaches ∞, x tends to 0. Additionally, the definition of the displacement function in the frequency domain can be used to further simplify the integral term

$$2\xi\omega_n^2 \int_\infty^\infty \dot{x}e^{-i\omega t}dt = 2\xi\omega_n^2(i\omega)X(\omega). \tag{4.18}$$

Lastly, the integral containing the acceleration variable, $\ddot{x}$ can be solved by parts as well:

$$\ddot{x}e^{-i\omega t}dt = \left(\frac{dx(t)}{dt}e^{-i\omega t}\right)\Big|_\infty^\infty - (i\omega)\int_\infty^\infty \dot{x}e^{-i\omega t}dt.$$

Similar to the previous solution, the first term will approach 0 when it is evaluated between $[-\infty, \infty]$. The second term was solved previously, leading to the following expression

$$\int_\infty^\infty \ddot{x}e^{-i\omega t}dt = -\omega^2 X(\omega). \tag{4.19}$$

In terms of the frequency dependent force

$$F(\omega) = \int_\infty^\infty [F_0 sin(\omega t)]e^{-i\omega t}dt. \tag{4.20}$$

By substituting equations (4.17), (4.18), (4.19) and (4.20) into equation (4.14)

$$\frac{\omega_n^2}{k}F(\omega) = -\omega^2 X(\omega) + i\omega(2\xi\omega_n)X(\omega) + \omega_n^2 X(\omega), \tag{4.21}$$

and solving for $X(\omega)/F(\omega)$

$$\frac{X(\omega)}{F(\omega)} = \frac{1}{k}\left[\frac{\omega_n^2}{-\omega^2 + i\omega(2\xi\omega_n) + \omega_n^2}\right]. \tag{4.22}$$

In regards to formulating and expression for the acceleration in the frequency domain, the acceleration term $\ddot{X}(\omega)$, is related to the displacement by a factor of ω^2 as can be seen in equation (4.19)

$$\frac{\ddot{X}(\omega)}{F(\omega)} = \frac{1}{k}\left[\frac{-\omega^2\omega_n^2}{-\omega^2 + i\omega(2\xi\omega_n) + \omega_n^2}\right). \tag{4.23}$$

4.3 Methods

4.3.1 Frequency Analysis of Head Impacts Delivered to Football Players

Analysis of Head Impacts in Human Subjects and Anthropomorphic Test Device

Before evaluating the performance of the helmets through the transmissibility and mechanical impedance parameters, two sets of data were recollected. The first, was the use of wearable sensors fitted on high school football players, with the goal of determining a FROI for head acceleration events (HAE). The second consisted in impacting a helmeted and unhelmeted 50th percentile male Hybrid III head form with a modal impact hammer.

xPatch (X2 Biosystem; Seattle, WA) wearable sensors were utilized to record HAE during training sessions that involved the use of personal protective equipment. These were placed on the right mastoid process - an anatomical landmark found as a prominence behind the ear - of each player and secured with adhesive tape [44]. The xPatch sensors have an integrated tri-axial accelerometer that allowed to measure impacts experienced to the head. Events that exceeded a value of $10g$, in any axes, were registered as HAEs. Following this, the Head Impact Monitoring System software (X2 Biosystems; Seattle, WA) was used to download the data after each practice session.

In terms of the Hybrid III head form, the acceleration data was registered by means of an array of accelerometers placed at the center of mass of the head form. A helmeted and unhelmeted head form was utilized throughout testing. A total of 5 locations were impacted, including: front, front-boss, side, rear-boss and rear. Five preset ranges of impulse were established for testing; $2 - 4Ns$, $4 - 7Ns$, $8 - 10Ns$, $11 - 14Ns$ and greater than $14Ns$. A rubber-tip modally tuned short-sledge impulse hammer (Model 086D20, PCB Piezotronics Inc.; Depew, NY) was used to deliver the impacts to the head form. The impulse hammer and accelerometer voltages

were digitized using a model 9234 data acquisition module (NI, Austin, TX) paired with custom software with a sampling frequency of 5120 Hz. A modified exponential windows was used to diminish the leakage, by focusing on the fact that the measured response tends to the noise of the ambient. Data recordings were processed by using kinematic equations to solve for angular acceleration and generate Peak Translational and Peak Angular Accelerations at the CoM using a custom Matlab code. [60].

Data Processing of in-game and simulated impacts

Matlab was used to transform the acceleration data collected from the X2 sensors from the time domain to the frequency domain. The *findpeaks* function was used to identify the maximum peak of the acceleration signal within the frequency response curve of the impact. An average was calculated, corresponding to the average peak acceleration over the total number of impacts per team participating in the study.

The unhelmeted head form was impacted 2400 times. For the helmeted system 1200 impacts were processed. Similar to the data processing for the xPatch sensors, the peak accelerations were identified. Lastly, peak accelerations were averaged for each of the impulse groups used through testing.

Data recorded through the accelerometers in the time domain was processed and transferred to the frequency domain. A fast Fourier transform was performed in Matlab for the transformation. Consequently, an algorithm was developed that would identify the maximum peak as a function of frequency of each HAE. In other words, it is possible to locate the peak linear acceleration of individual impacts. Data processing of HAEs was executed for all three participating teams. Furthermore, 75% of the area under the response curve was delimited as the FROI due to its biomechanical relevance. In total, 12582 were processed through the algorithm.
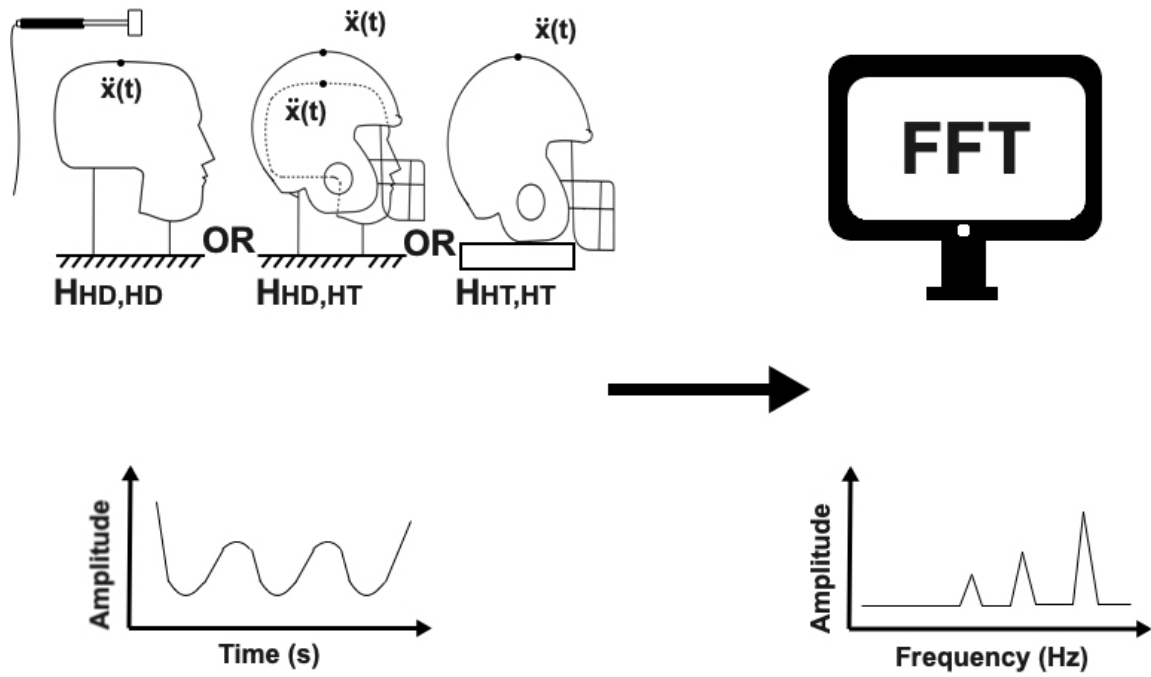
Fig. 4.3. Logic diagram showcasing how the time domain measurements for force and acceleration were taken and later on converted into a frequency domain signal through a fast Fourier transform algorithm. Force data was collected by means of the impulse hammer. Accelerometers were used for acceleration data in different component and system scenarios.

4.3.2 Experimental Determination of Transmissibility and Mechanical Impedance Model

Experimental Setup

A 2 component system was utilized to record the output and input of interest. The acceleration was registered by means of an array of tri-axial accelerometers (PCB Piezotronics Inc.; Depew, NY) arranged in a 3-2-2-2 formation within the center of mass of a Hybrid III 50th percentile head (Humanetics, Michigan). The head was at-

tached to an $82kg$ steel block through a Hybrid II 50th Percentile neck model. On the other hand, the input force of every individual strike was recorded through a rubber-tip modally tuned short-sledge impulse hammer (Model 086D20, PCB Piezotronics Inc.; Depew, NY). Voltage data from the accelerometers and impulse hammers were digitized by a 9234 data acquisition module (NI, Austin, TX) while being coupled to a software that would allow for a sampling frequency of $5120Hz$ (Fig. 4.3). An algorithm was developed in Matlab that would: 1) process the data inputs and outputs by using kinematic equations; 2) obtain peak translational and peak angular acceleration at the center of mass by solving the kinematics for angular acceleration.
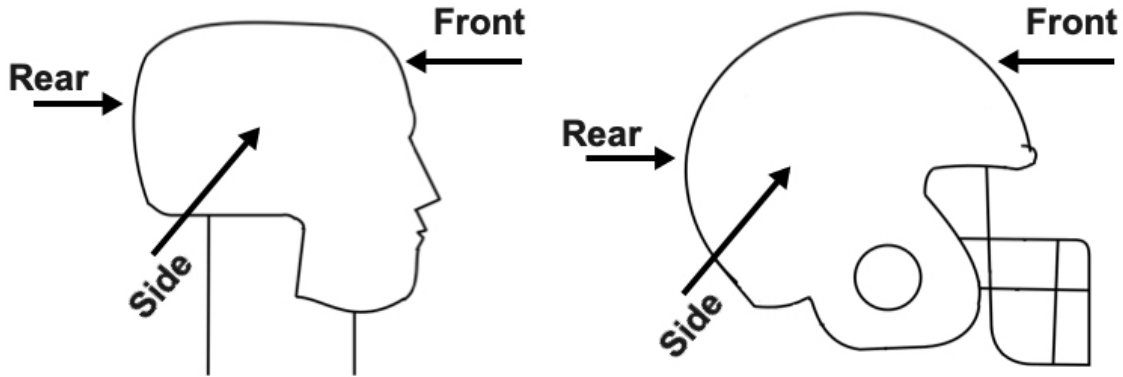
Fig. 4.4. Visual representation of the impact locations determined on both the unhelmeted Hybrid III 50th head form and helmeted head form. The three locations chosen were rear, front and side. Only the right side was hit during test, under the assumption that both the left and right sides would have the same response when impacted.

Data Collection

The design of the experiment allowed for data recollection of the mechanical impedance and transmissibility of the helmet and its padding. Xenith X1 (Xenith;

Detroit, MI) and Schutt Ion (Schutt Sports; Litchfield, IL) helmets were used for testing. Two configurations were used during impact testing: component and system. During component trials, a uni-axial accelerometer was either adhered to the outer surface of the helmet or the most superficial layer of the Hybrid III head form. For system tests, two accelerometers were used. The first was placed on the outer shell of the helmet. The second accelerometer was aligned with the first, however, was mounted on the outer surface of the head form. The acceleration sensors were positioned in the front, right side (symmetry was assumed for the response between the right and left side of the head from) and the rear (Figure 4.4). The modally tuned short-sledge impulse hammer was the tool used to impact each location, making sure it recored hits between the range $100 - 200 lbforce$.

4.3.3   Quantification of Transmissibility and Mechanical Impedance

Transmissibility Quantification

The necessary acceleration data was obtained by means of the coupled system between the head form and helmet. The three locations mentioned in prior instance were impacted five times by the impulse hammer, making sure the strike was as close to the accelerometer as possible. The acceleration response was recorded by each accelerometer and a FFT algorithim was used to transform the data into the frequency domain (Figure 4.3). As a last step, the transmissibility was calculated according to equation (4.1) by taking the ration of the output acceleration, $\ddot{X}_{HD}(\omega)$, to the input acceleration, $\ddot{X}_{HT}(\omega)$. The importance of calculating the transmissibility relies in the fact that it allows to understand the relative acceleration the head feels in comparison to the helmet when excited by an external force, the modal hammer in this case. The nature of the relationship between the input and output can be inferred by comparing to transmissibility unity, given that the calculated value is a ratio. If the value of the transmissibility is equivalent to one, both objects of interest experienced the same acceleration for a given force. If the transmissibility was greater

than one, the resultant acceleration of the head was larger than that experienced by the head. This can be interpreted as an amplification of the input force. If the calculated transmissibility is less than one, the acceleration experienced by the head was less than the acceleration of the helmet for a given force. In other words, there was an attenuation of the force.

Mechanical Impedance Experimental Measurement

Given the need to calculate FRFs for the head and helmet in different scenarios, both the component and system level tests were used. The component level test would allow for the acquisition of the uncoupled FRF for the head, $H_{HD,HD}$, and helmet, $H_{HT,HT}$. In the interest of obtaining the uncoupled response of the head, strikes were dealt to the bare Hybrid III head form set on the steel block. Helmet-wise, $H_{HT,HT}$ was obtained by placing the helmet on a block of soft foam and imapacting it with the impulse hammer. In regards to the system level testing, a coupled response between the head and helmet, $H_{HT,HD}$, was experimentally obtained. In this case, blows were dealt while the helmet was secured on the head form. It is worth mentioning that the tension of the straps was not measured, they were merely adjusted according to the user's manual before impacts. Moreover, special attention was paid to carefully mounting the helmet on the head without dislodging any of the accelerometers.

It is important to note that $Z(\omega)$ was quantified through the experimentally obtained values of the FRFs. In other words, equation 4.2 was used as theoretical formulation to further understand the relationship between the input force and output acceleration being measured during experimental procedures to obtain the FRFs. Nonetheless, in reality, the estimator of the frequency response function was calculated by means of the cross spectral (G_{XY}) and auto spectral density (G_{YY}) functions of the parameters of interest.

$$H(\omega) = \frac{G_{XY}}{G_{YY}}. \tag{4.24}$$

The auto spectral density is a measure of the power over a given range of frequency. Cross spectral density is a function that allows to identify the linear relationship between Y (output acceleration) and X (input force). A command in Matlab was used to calculated both the auto and power spectral densities. The reason to utilize this practical definition is to account for the noise on the input variable. Noise in the input signal is random variation that can be inherent to the sensor or accounted for by mechanical input unrelated to the experiment, picked up by the sensor.

4.4   Results

4.4.1   Biomechanical frequency range of interest

Acceleration data of the HAEs taken from the time domain downloaded through the xPatch and were transformed to the frequency domain (Figure 4.5). The data transformed through an FFT contains a gray shaded area which represents 75% of the area of the total signal. The upper boundary of the FROI for the event is equivalent to the frequency range at the 75% mark. Table 4.1 shows the frequency rang of interest per participating team that range from $0 - 200Hz$. When it comes to the peak acceleration, the average frequency at which it was found ranged between $8.92 - 11.22Hz$ for all recorded impacts.

Having determined a biomechanical FROI for in-game HAES, the acceleration data for the simulated impacts recorded on the unhelmeted Hybrid 3 headform was constrained to this range (Figure 4.6). The smallest impulse range, corresponding to $2 - 4Ns$ averaged values of $17.22g \pm 20.86g$ which translates to a HAE of $244.26N \pm 252.22N$. On the other hand, for the highest impulse range of $> 14Ns$, the accelerations registered of $191.70g \pm 23.31g$ corresponded to a force of $2270.51N \pm 240.79N$ (Table 4.2). The peak accelerations in the frequency domain ranged between $1.35Hz \pm 0.65Hz$ and $5.83Hz \pm 0.52Hz$. Large impact forces, with resultant peak accelerations, occurred at higher frequencies than those peaks that were measured at lower impact forces.
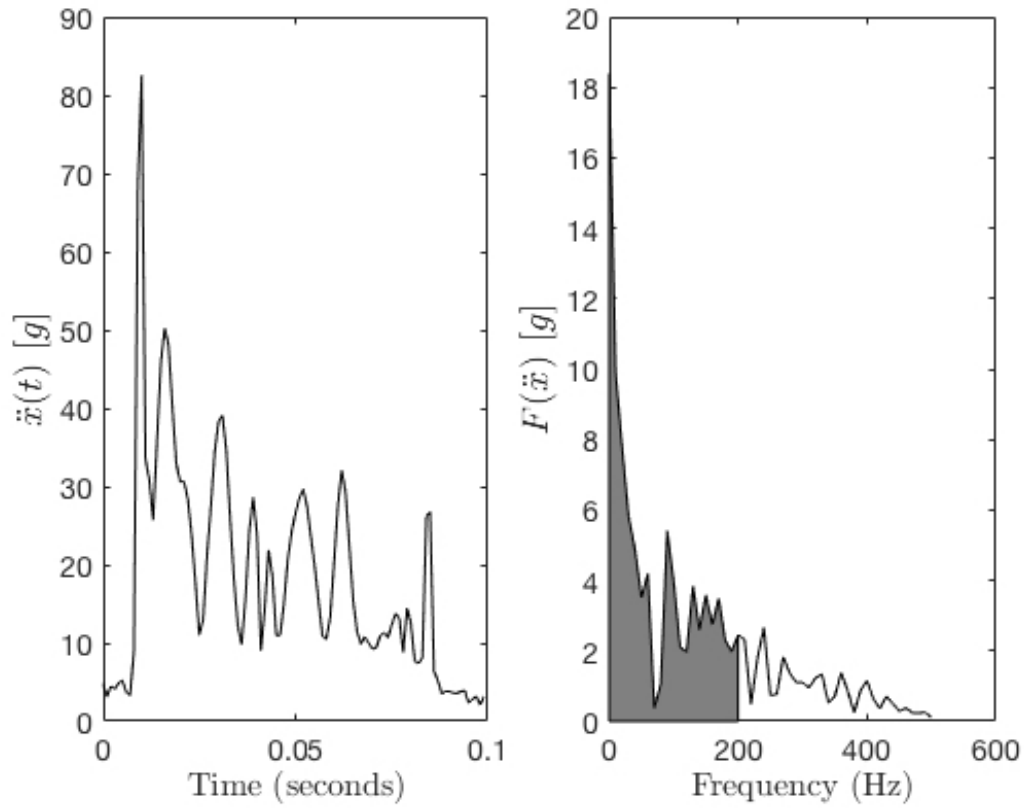
Fig. 4.5. HAE wave form extracted from data recollected from a Football player in Team 1 utilizing the xPatch sensor. a) Data in the time domain, despite being noisy, a peak in acceleration is evident. b) Frequency domain data, post-FFT, in which an area shaded in gray is identified as 75% if the total area of the signal.

Table 4.1.

The recordings correspond to in-game impacts for 3 high school teams, for a total of 12582 impacts. Acceleration data in the time domain was obtained from the xPatch sensors and converted to the frequency domain impacts. Peak acceleration for each impact was located and averaged for each participating team. A frequency range of interest was determined by calculating 75% of the area under the curve and indexing its frequency.

Team No.	No. of Hits	Frequency at Peak Acceleration [Hz] Mean ± St. Dev.	Frequency Range of Interest [Hz] Upper Boundary
1	2912	11.22 ± 6.85	198
2	5336	9.81 ± 6.34	200
3	4334	8.92 ± 5.59	195

By introducing a helmet in the system, a reduction in force and peak acceleration was seen in both the time (Figure 4.6) and frequency domain (Figure 4.6).

4.4.2 Transmissibility

As mentioned in prior instance, transmissibility unity is the point of reference. That said, at 0 Hz the transmissibility should have a value of 1, given that the head form is not moving.. For the location of the forehead (Figure 4.7a), below the 40Hz mark there is noticeable variability. Helmets from the Schutt brand have a clear peak at 10Hz, in contrast to the results seen from the Xenith helmet, which do not exceed unity for any frequency value throughout testing.

A marked distinction is evident below and above 60Hz for data corresponding to impacts dealt to the rear of the helmets (Figure 4.7c). Above 60 Hz, the transmissibility is close to a value of 0. Below the 60Hz mark, the data is higher than transmissibility unity which can be interpreted as an amplification of the signal, and force from the helmet to the head.

It is clear that helmets manufactured at Xenith do not perform well when struck at the right side location (Figure 4.7e). Around the 15 and 20Hz mark, there are

61
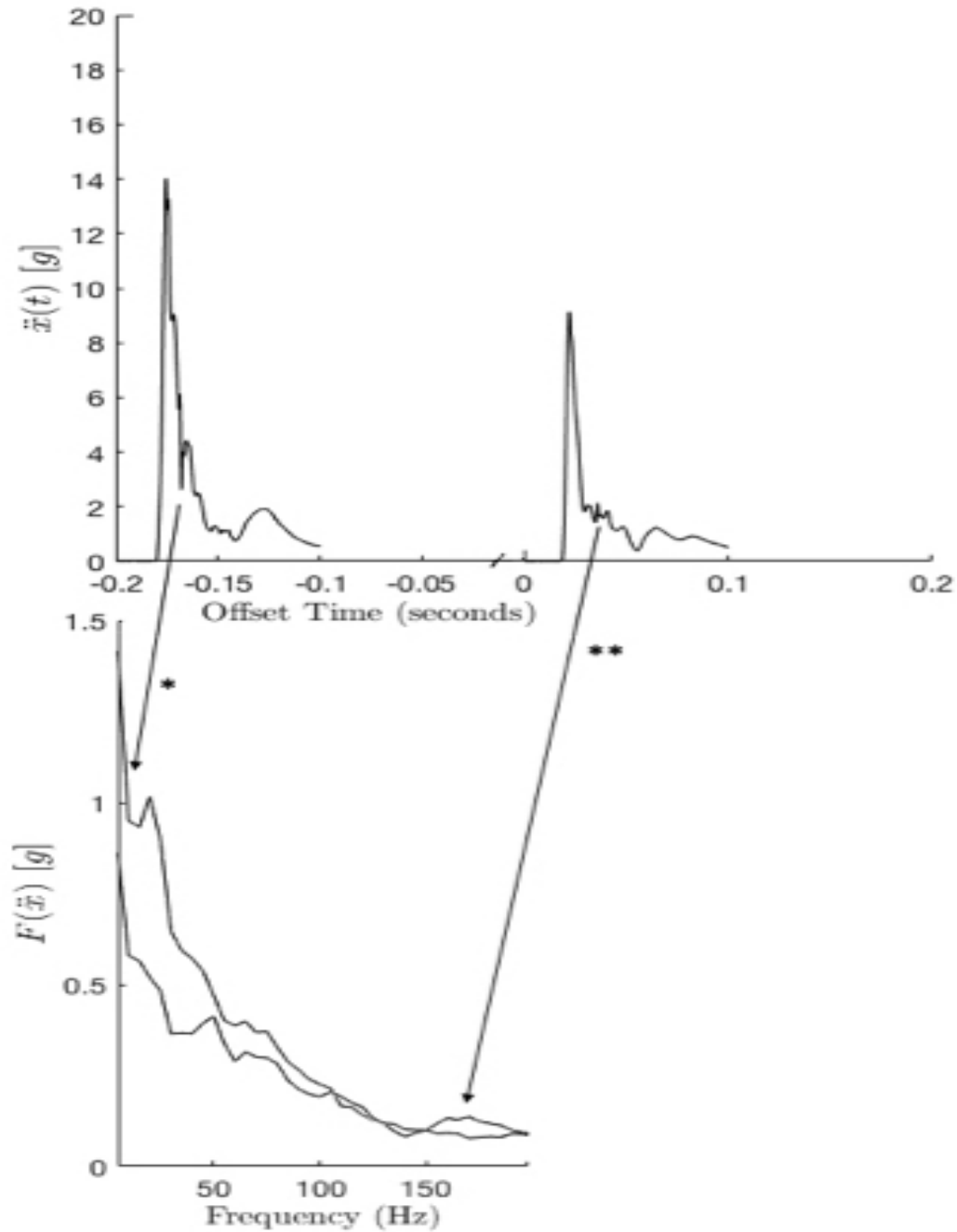
Fig. 4.6. Top graph corresponds to acceleration data in the time domain after striking bot the unhelmeted Hybrid 3 head form (*) and helmeted head form (**). Acceleration data in the frequency domain for both helmeted and unhelmeted headforms is present in the bottom graph. Acceleration recorded in the time domain is plotted for an approximate duration of 0.1s. The frequency domain data is constrained to the FRO (0-200Hz) determines through the xPatch data analysis.

Table 4.2.

Comparison of peak acceleration and force, in both the time and frequency domain, for the 5 pre-determined impulse ranges. Data for the unhelmeted head form corresponds to 240 hits per impulse range, for a total of 1200 impacts. On the other hand, 480 hits were recorded per impulse range, for a total of 2400 wave forms for the coupled helmet-head system.

Impulse Range [Ns]	Unhelmeted Hybrid III Head Form		Helmeted Hybrid III Head Form	
	Peak Acceleration [g] Mean ± St. Dev.	Frequency at Peak Acceleration [Hz] Mean ± St. Dev.	Peak Acceleration [g] Mean ± St. Dev.	Frequency at Peak Acceleration [Hz] Mean ± St. Dev.
2-4	17.22±20.86	1.35±0.65	8.65±4.36	0.99±0.32
5-7	37.28±13.69	2.31±0.54	16.89±5.01	1.69±0.43
8-10	68.56±20.25	3.32±0.62	23.57±6.95	2.31±0.53
11-13	129.84±28.84	4.70±0.65	31.88±8.32	2.99±0.56
13¡	191.70±23.21	5.83±0.52	44.30±14.00	3.67±0.60

transmissibilty values above 1. In terms of Schutt helmets, there was poor performance around the 15 and 22 Hz frequency values. Nonetheless, these peaks are short and not sustained regions of response. The transmissibility tends to a value of 0 at approximately the 60Hz mark.

4.4.3   Model for the Mechanical Impedance

In accordance to the theoretical formulation of the mechanical impedance, a lower value of $Z(\omega)$ is advisable. This due to the fact that it translates to a less couples response of the head when being impacted by force at the helmet.

In terms of the forehead location (Figure 4.7b), there was not a desireable performance below the 100 Hz mark. Elevated values of $Z(\omega)$ were observed below 40Hz, with a clear peak at 26Hz for the Xenith helmets. This location has noticeably higher values of the impedance when compared to the other two regions.

A similar behavior was observed in the rear location (Figure 4.7d), where the stabilization of $Z(\omega)$ happened around the 55Hz mark. Schutt had higher values of impedance when compared to Xenith. A steeper drop was seen for Xenith helmets after the peak at 37Hz.

For the side location, both football helmets had a poor overall performance, with high impedance values seen across the spectrum (Figure 4.7f). The stabilization of $Z(\omega)$ occurs at a frequency above 130Hz.

4.5   Discussion

The frequency domain analysis derived and implemented herein combined field data to determine the frequency spectra of head impacts in high school football with a set of modal hammer-based impact measurements to quantify the dynamic characteristics of football helmets. Unfortunately, data from both helmet models exhibited transmissibilities well above one in the 0-40 Hz range with the magnitude characteristics varying considerably with the location of the impact. The impedance, , also
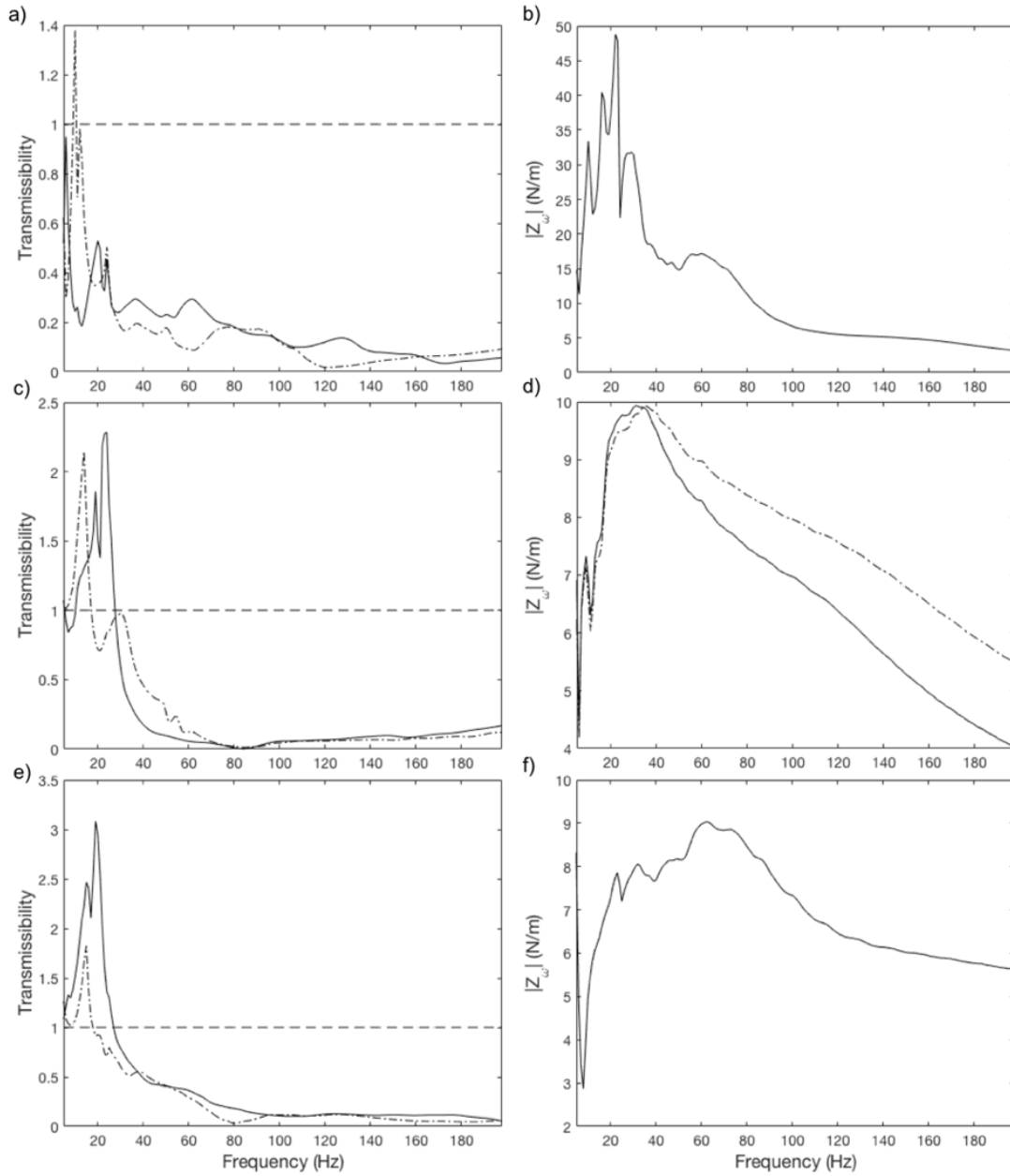
Fig. 4.7. Average transmissibility and mechanical impedance are plotted against frequency in Hz for the Shutt and Xenith helmets. Schutt (dash-dot) and Xenith (solid) were impacted in locations: forehead (a,b), rear (c,d) and right side (e,f). Several peaks below unity - force amplification - are seen across the locations under 40Hz frequencies for the transmissibility of both helmets. Alike, high values of the mechanical impedance are found in the same range, which indicates poor performance.

depended on impact location, ranging from 9 on the side of the helmet to almost 50 at the top front. These data suggest that, in addition to mitigating skull fractures, new helmet designs should focus on absorbing energy, especially in the low frequency domain.

Despite testing helmets from two different manufacturers, the trends observed were comparable, suggesting that current helmet designs are unable to sufficiently mitigate impacts across the range of frequencies observed in game situations. To date, helmet characterization has been primarily performed on helmets without facemasks using a drop tower-based standard [21] that was designed to ensure that the helmet could protect against skull fracture or other forms of severe brain trauma. More recent standards employ pneumatic rams, but utilize the same injury criterion [21] [77]. Combining these methods with a frequency domain analysis such as the one proposed here may provide an algorithm for characterizing and designing helmets capable of mitigating brain injuries of all types.

This technique makes it possible to measure a number of frequency domain parameters that provide a means of selecting materials and geometries that will maximize the attenuation of the impact load. In order to reduce the risk of TBI in athletes participating in contact sports the transmissibility and mechanical impedance have to be considered as design factors.

There are several limitations of the current study. Firstly, the frequency range of interest was overestimated as a safety factor. The FFT taken from the xPatch sensors was transforming the magnitude of the raw acceleration data collected. Ergo, higher frequency components - two-fold minimum - were introduced into the signals. Second, the range of impacts captured between the xPatch and the Hybrid III system differ slightly. While the frequency responses were generally comparable, it is important to note that the precise forces experienced during in-game impacts are unknown and cannot be determined solely from the kinematic relationship [60]. Thirdly, we only report a single transmissibility value at each location. In order to fully characterize the behavior of each component of the system, transmissibilities should be quantified

between the impact location and multiple points on the head. This would require a model much more biofidelic than the Hybrid III system. Lastly, the impedance model presented in section 2.2 assumes a linear relationship between the padding and the shell of the helmet. Future work should consider nonlinear force-deflection profiles in an effort to better understand the design parameter space for helmets and other protective gear.

Future studies should focus on how modifying a helmets geometry or padding systems will directly affect the frequency-domain parameter measurements. The goal is to optimize the design so that there is a reduction of the transmissibility and mechanical impedance across a range of head impacts. This should result in a measurable level of mitigation of the deleterious effects of TBI in athletes. It should be noted, however, that such data can only be obtained currently through biomedical imaging-based studies [7] [73] [5]. This methodology should make it possible to obtain a reasonable range for the mechanical impedance.

5. CONCLUSION

Velocity of incoming soccer balls and their pressure of inflation were determined as two of the most influential factors affecting the peak impact force of soccer kicks. Due to the nature of the game, some of these balls will be in contact with athletes heads as it is used as a tool in the game. The resulting peak linear acceleration experienced by the head after being in contact with the soccer ball has been found to result in neurocognitive impairment. Thus, a more extensive control on parameters such as the inflation pressure and headers during game-play should allow for a safer environment for soccer players.

Soccer headbands that were manufactured and tested showed potential to decrease peak translational acceleration in impacts. The use of a two-layered system that included silicone padding and a carbon fiber shell out-performed existing commercial headbands within a clinically relevant range.

A vast majority of the head acceleration events were located within a frequency range of interest of 0 - 200 Hz. The transmissibility and mechanical impedance, two frequency domain parameters, were introduced to evaluate the performance of helmets and aid in the improved manufacturing of helmets to reduce the risk of traumatic brain injury in athletes. As a result of the underperformance of the coupled head-helmet systems at low frequencies, it is important to lower both the mechanical impedance and transmissibilty of the system.

6. RECOMMENDATIONS, LIMITATIONS AND FUTURE WORK

6.1 Recommendations

Governing bodies within the soccer world should not only acknowledge the existence of traumatic brain injuries, but work to combat, prevent and treat them properly. The study that took place highlighted some of the parameters that are directly affecting the incidence of TBI incidents related to heading a soccer ball. Appropriate enlightenment to all participants in soccer is necessary through different media, whether its reports, conferences or q/a sessions. Special attention should be drawn to the inflation pressure of soccer balls. Controlling the pressure and enforcing that its value is kept closer to the lower boundaries of what is stipulated in-game should be a priority. The simple use of a digital pressure gauge before games and during half-time is a step in the right direction. Referees and coaches should be required to utilize these more often, and even suggest that their players carry them as part of their equipment kit. Moreover, female leagues should transition into the use of size 4.5 soccer balls. Despite their not being a large difference between the mass of the size 5 and 4.5 balls, the peak impact force can be reduced. The former recommendations do not deeply impact the nature of the game and can easily be adopted by players and leagues across different levels of play. More fundamental changes of the game include altering certain game conditions and legal action against ball manufacturers. Output from the sensitivity analysis allowed to conclude that the velocity is the most influential factor when it came to the value of peak impact force. Ergo, forbidding players to header balls coming from goal-kicks is a desired scenario, given that these are associated to high velocities. In terms of possible legal action, soccer ball manufacturers should be more mindful of enforcing that product users maintain pressures

specified on their balls. Moreover, they have the capacity of modifying the pressure range imprinted on their balls with the basis of preventing TBI.

Headgear-wise, a series of recommendations can be presented. Players of certain age-grades should be obliged to use headgear in game and during practice, no matter what type of headgear. Despite existing commercial headbands not performing well across the entire range of forces experienced in simulated environments, they do manage to mitigate the impact forces. In addition, an age restriction should be put in place for when athletes are allowed to partake in plays associated to heading. Transitioning to football, a more holistic evaluation of protective headgear utilized within the sport should take place. Modern day helmet manufacturers should ensure that their products are keeping their users safe. In order to do so, alternative certification programs should be established that focus on the mitigation of subconcussive impacts.

6.2 Limitations and Future Work

6.2.1 Soccer Ball Parameter Characterization

The first major limitation of the study was the fact that the kicks being recorded were being delivered by an athlete. In other words, kicks were not consistent and a noteworthy amount were discarded due to the ball ricocheting. In addition, even if they were not disregarded, tracking of the soccer balls after an angled deflection was arduous. Secondly, the video resolution and quality was not the highest. Having video clips with a larger set of frames would increase the fidelity of the velocity values obtained through the tracking software. Being limited to 240 frames per second constrained the velocity measurements obtained.

For future reference, different kinds of kicks could be used. In spite of an instep kick technique being preferred due to its capacity of reaching higher peak forces, repeatability is concerning. However, this may also be cause by the use of an athlete and not a machine to deliver the soccer balls. A launcher would be a suitable re-

placement, more so if the velocity can be preset beforehand. Furthermore, it would be beneficial to understand what genuine in-game forces or accelerations by securing wearable sensors and obtaining medical images of athletes during practice sessions and official games throughout a season. By following a team it would be possible to modify game-play and understand how changes in pressure inflation, laws of the game or size of the ball affect soccer players.

6.2.2   Innovative Headgear for use in Soccer

Manufacturing of the soccer headbands was limited by different factors. Firstly, the design of the mold was restricted to a 50th percentile male. Tailor-made headgear would only be useful for a restricted amount of users. In addition, the use of the B-rep geometry resulted in a negative impression that was not as smooth as desired. The accuracy of the mesh, and consequent CAM model, was ensued by the post-processing procedure. Secondly, the wooden molds limited the type of manufacturing process that could be used to manufacture the headbands. Room temperature curing of epoxy resins results in a low transition glass temperature and as a consequence, less optimum mechanical properties. However, heat curing - that should yield a higher T_G - was not an option with a wooden molds that would: 1) combust inside an autoclave or 2) morph due to the interaction between heat and the material. In third place, a wet layup procedure does not ensure a uniform distribution of epoxy across the fabric being used, easily leading to dry-spots and other weaknesses of the product. Lastly, the adhesion between the padding and composite shell was fragile, which has implications at the moment of testing the headgear on the Hybrid III head.

Future work in regards to the headband includes: use of different padding geometries; improved methods for manufacturing composite materials and on-field testing of the product. The padding utilized during testing was kept to a simple geometry that would easily comply with having three degrees of porosity. Distinct geometries can be used that would fit an athletes head better and have a better adhesion in-

terface with the composite shell. As mentioned in prior instance, there are several improvements that can be made including using a composite material tool that will allow for heat curing of the epoxy resin and the use of prepeg epoxy instead of a wet layup for a more homogeneous distribution of the resin. Lastly, although the performance of the product was satisfactory within the confines of the testing environment, on-field testing is required. Composite shells are primarily seen on soccer players as a tool to help them in their recuperation process of a facial fracture, not in headbands. Encouraging players to utilize these composite-based products would allow to see how deeply it can impact traditional game-play.

6.2.3 Frequency Domain Analysis for Protective Headgear

Whilst performing the frequency analysis, one of the most important limitations being faced was the fact that the FROI was overestimated. Additionally, the model being proposed is linear and might not reflect the reality of the problem. A non-linear force-deflection profile describing the interactions between the padding and the composite shell is probably more genuine.

As a means to further improve the analysis, more locations should be tested. During the evaluation of the helmets, only three locations were observed - front, rear and side. However, other certification protocols require testing in other locations such as the front-boss, rear-boss and top of the helmet. Another aspect that could be improved in the future would be the calculation of other types of transmissibilities. During the study, the an overall transmissibility was quantified that was based on the interface between the entire helmet and the head. Nevertheless, there is interlinkage of other components of the system such as the helmet shell and the padding, or the padding and the head. It would be useful to know how force is being distributed among these surfaces to further improve the design of both the shell, helmets and their adhesion. Additional to that, a wider variety of helmets has to be tested in order to have a larger data set to validate the evaluation method.

REFERENCES

REFERENCES

[1] Centers for Disease Control and Prevention, "Morbidity and Mortality Weekly Report Centers for Disease Control and Prevention MMWR Editorial and Production Staff MMWR Editorial Board," Tech. Rep. 39, 2011. [Online]. Available: https://www.cdc.gov/mmwr/pdf/wk/mm6039.pdf

[2] C. S. Sahler and B. D. Greenwald, "Traumatic Brain Injury in Sports: A Review," *Rehabilitation Research and Practice*, vol. 2012, pp. 1–10, 2012. [Online]. Available: https://www.ncbi.nlm.nih.gov/pmc/articles/PMC3400421/pdf/RERP2012-659652.pdf

[3] P. McCrory, W. Meeuwisse, J. Dvorak, M. Aubry, J. Bailes, S. Broglio, R. C. Cantu, D. Cassidy, R. J. Echemendia, R. J. Castellani, G. A. Davis, R. Ellenbogen, C. Emery, M. Putukian, K. J. Schneider, A. Sills, C. H. Tator, M. Turner, and P. E. Vos, "Consensus statement on concussion in sport-the 5 th international conference on concussion in sport held in Berlin, October 2016 Consensus statement," *British Journal of Sports Medicine*, vol. 0, pp. 1–10, 2017. [Online]. Available: http://bjsm.bmj.com/

[4] K. M. Breedlove, E. L. Breedlove, M. Robinson, V. N. Poole, J. King, P. Rosenberger, M. Rasmussen, T. M. Talavage, L. J. Leverenz, and E. A. Nauman, "Detecting Neurocognitive and Neurophysiological Changes as a Result of Subconcussive Blows Among High School Football Athletes," *Athletic Training & Sports Health Care*, vol. 6, no. 3, pp. 119–127, 2014.

[5] T. M. Talavage, E. A. Nauman, E. L. Breedlove, U. Yoruk, A. E. Dye, K. E. Morigaki, H. Feuer, and L. J. Leverenz, "Functionally-Detected Cognitive Impairment in High School Football Players without Clinically-Diagnosed Concussion," *Journal of Neurotrauma*, vol. 31, pp. 327–338, 2014. [Online]. Available: www.nfhs.org

[6] D. O. Svaldi, E. C. Mccuen, C. Joshi, M. E. Robinson, Y. Nho, R. Hannemann, E. A. Nauman, L. J. Leverenz, and T. M. Talavage, "Cerebrovascular reactivity changes in asymptomatic female athletes attributable to high school soccer participation," *Brain Imaging and Behavior*, vol. 11, no. 1, pp. 98–112, 2017. [Online]. Available: https://link.springer.com/content/pdf/10.1007/s11682-016-9509-6.pdf

[7] E. L. Breedlove, M. Robinson, T. M. Talavage, K. E. Morigaki, U. Yoruk, K. O'keefe, J. King, L. J. Leverenz, J. W. Gilger, and E. A. Nauman, "Biomechanical correlates of symptomatic and asymptomatic neurophysiological impairment in high school football $," *Journal of Biomechanics*, vol. 45, pp. 1265–1272, 2012. [Online]. Available: www.elsevier.com/locate/jbiomech

[8] J. J. Bazarian, T. Zhu, J. Zhong, D. Janigro, E. Rozen, A. Roberts, H. Javien, K. Merchant-Borna, B. Abar, and E. G. Blackman, "Persistent, Long-term

Cerebral White Matter Changes after Sports-Related Repetitive Head Impacts," *Plos One*, vol. 9, no. 11, pp. 1–12, 2014. [Online]. Available: www.plosone.org

[9] B. I. Omalu, S. T. Dekosky, R. L. S. Minster, M. I. Kamboh, R. L. Hamilton, and C. H. Wecht, "CHRONIC TRAUMATIC ENCEPHALOPATHY IN A NATIONAL FOOTBALL LEAGUE PLAYER," *Neurosurgery*, vol. 57, no. 1, pp. 128–134, 2005. [Online]. Available: https://academic.oup.com/neurosurgery/article-abstract/57/1/128/2743944

[10] J. Mez, D. H. Daneshvar, P. T. Kiernan, B. Abdolmohammadi, V. E. Alvarez, B. R. Huber, M. L. Alosco, T. M. Solomon, C. J. Nowinski, L. McHale, K. A. Cormier, C. A. Kubilus, B. M. Martin, L. Murphy, C. M. Baugh, P. H. Montenigro, C. E. Chaisson, Y. Tripodis, N. W. Kowall, J. Weuve, M. D. McClean, R. C. Cantu, L. E. Goldstein, D. I. Katz, R. A. Stern, T. D. Stein, and A. C. McKee, "Clinicopathological Evaluation of Chronic Traumatic Encephalopathy in Players of American Football," *JAMA*, vol. 318, no. 4, pp. 360–370, jul 2017. [Online]. Available: http://jama.jamanetwork.com/article.aspx?doi=10.1001/jama.2017.8334

[11] B. I. Omalu, R. P. Fitzsimmons, J. Hammers, and J. Bailes, "Chronic traumatic encephalopathy in a professional American wrestler," *Journal of Forensic Nursing*, vol. 6, pp. 130–136, 2010. [Online]. Available: https://onlinelibrary.wiley.com/doi/pdf/10.1111/j.1939-3938.2010.01078.x

[12] H. Ling, H. Morris, J. Neal, A. Lees, J. Hardy, J. Hotlon, T. Revesz, and D. Williams, "Chronic Traumatic Enecephalopathy in Retired Footballers with Dementia," *Journal of Neurology, Neurosurgery and Psychiatry*, vol. 88, p. A1, 2017.

[13] L. Gessel, F. Sarah, C. Collins, R. Dick, and D. Comstock, "Concussions Among United States High School and Collegiate Athletes," *Journal of Athletic Training*, vol. 42, no. 4, pp. 495–503, 2007.

[14] R. D. Comstock, D. W. Currie, L. A. Pierpoint, J. A. Grubenhoff, and S. K. Fields, "An Evidence-Based Discussion of Heading the Ball and Concussions in High School Soccer," *JAMA Pediatrics*, vol. 169, no. 9, p. 830, sep 2015.

[15] M. L. Levy, A. S. Kasasbeh, L. C. Baird, C. Amene, J. Skeen, and L. Marshall, "Concussions in Soccer : A Current Understanding," *World Neurosurgery*, vol. 78, no. 5, pp. 535–544, 2012.

[16] J. W. O. Kane, A. Spieker, M. R. Levy, M. Neradilek, N. L. Polissar, and M. A. Schiff, "Concussion Among Female Middle-School Soccer Players," *Journal of American Medical Association Pediatrics*, vol. 168, no. 3, pp. 258–264, 2014.

[17] C. Withnall, N. Shewchenko, M. Wonnacott, and J. Dvorak, "Effectiveness of headgear in football," *Br J Sports Med*, vol. 39, pp. 40–48, 2005. [Online]. Available: http://bjsm.bmj.com/

[18] K. M. Guskiewicz, M. McCrea, S. W. Marshall, R. C. Cantu, C. Randolph, W. Barr, J. A. Onate, and J. P. Kelly, "Cumulative Effects Associated With Recurrent Concussion in Collegiate Football Players," *JAMA*, vol. 290, no. 19, pp. 2549–2555, nov 2003. [Online]. Available: http://jama.jamanetwork.com/article.aspx?doi=10.1001/jama.290.19.2549

[19] K. Abbas, T. E. Shenk, V. N. Poole, E. L. Breedlove, L. J. Leverenz, E. A. Nauman, T. M. Talavage, and M. E. Robinson, "Alteration of Default Mode Network in High School Football Athletes Due to Repetitive Subconcussive Mild Traumatic Brain Injury :," *Brain Connectivity*, vol. 00, no. 00, 2014.

[20] K. Abbas, T. E. Shenk, V. N. Poole, M. E. Robinson, L. J. Leverenz, E. A. Nauman, and T. M. Talavage, "Effects of Repetitive Sub-Concussive Brain Injury on the Functional Connectivity of Default Mode Network in High School Football Athletes," *Developmental Neuropsychology*, vol. 40, no. 1, pp. 51–56, 2015. [Online]. Available: https://www.tandfonline.com/action/journalInformation?journalCode=hdvn20

[21] NOCSAE, "Standard Perfoemance Specification for Newly Manufactured Football Helmets," 2017.

[22] FIFA, "FIFA Big Count 2006: 270 million people active in football," Tech. Rep., 2007. [Online]. Available: https://www.fifa.com/mm/document/fifafacts/bcoffsurv/bigcount.statspackage_7024.pdf

[23] M. Aubry, R. Cantu, J. Dvorak, T. Graf-Baumann, K. Johnston, J. Kelly, M. Lovell, P. McCrory, W. Meeuwisse, and P. Schamasch, "Summary and agreement statement of the first International Conference on Concussion in Sport, Vienna 2001," *British Journal of Sports Medicine*, vol. 36, no. 1, pp. 6–7, feb 2002. [Online]. Available: http://bjsm.bmj.com/cgi/doi/10.1136/bjsm.36.1.6

[24] AAPCSM, "American Academy of Pediatrics Committee on Sports Medicine: American Academy of Pediatrics policy statement: recommendations for participa- tion in competitive sports." *Phys Sportsmed*, vol. 16, no. 5, pp. 165–167, 1988.

[25] L. A. Keeler, "The Differences in Sport Aggression, Life Aggression, and Life Assertion Among Adult Male and Female Collision, Contact and Non-Contact Sport Athletes," *Journal of Sport Behavior*, vol. 30, no. 1, 2007. [Online]. Available: https://learnzone.loucoll.ac.uk/sportres/HE/HEStudySkills/Criticalanalysis/JournalarticlesfromPPAD20092010/the{_}differences{_}in{_}sport{_}aggression.pdf

[26] B. A. Tommasone and T. C. V. Mcleod, "Contact Sport Concussion Incidence," Tech. Rep. 4, 2006. [Online]. Available: www.journalofathletictraining.org

[27] B. P. Boden, D. T. Kirkendall, and W. E. Garrett, "Concussion Incidence in Elite College Soccer Players," *The Amer*, vol. 26, no. 2, pp. 238–241, 1998.

[28] B. C. Barnes, L. Cooper, D. T. Kirkendall, T. P. Mcdermott, B. D. Jordan, and W. E. Garrett, "Concussion History in Elite Male and Female Soccer Players," *The American Journal of Sports Medicine*, vol. 26, no. 3, pp. 433–438, 1998.

[29] R. S. Naunheim, J. Standeven, C. Richter, and L. M. Lewis, "Comparison of Impact Data in Hockey, Football, and Soccer," *The Journal of Trauma: Injury, Infection and Critical Care*, vol. 48, no. 5, pp. 48–51, 2000.

[30] R. S. Naunheim, A. Ryden, J. Standeven, G. Genin, L. Lewis, P. Thompson, and P. Bayly, "Does Soccer Headgear Attenuate the Impact When Heading a Soccer Ball ?" *Acad Emerg Med*, vol. 10, no. 1, pp. 85–90, 2003.

[31] C. F. Babbs, "Biomechanics of Heading a Soccer Ball: Implications for Player Safety," *The Scientific World*, vol. 1, pp. 281–322, 2001. [Online]. Available: http://docs.lib.purdue.edu/bmepubshttp://dx.doi.org/10.1100/tsw.2001.56

[32] NCAA, "Soccer 2018 and 2019 Rules," National Collegiate Athletic Association, Indianapolis, Tech. Rep., 2018. [Online]. Available: http://www.ncaapublications.com/productdownloads/SO19.pdf

[33] FIFA, "Laws of The Game 2015/2016," Tech. Rep., 2016. [Online]. Available: http://www.fifa.com/mm/Document/FootballDevelopment/Refereeing/02/36/01/11/LawsofthegamewebEN_Neutral.pdf

[34] K. Sakamoto, Y. Shimizu, E. Yamada, and S. Hong, "Difference in kicking motion between female and male soccer players," in *Procedia Engineering*, vol. 60, 2013, pp. 255–261.

[35] A. Kapidžic, T. Huremovi, and A. Biberovic, "Kinematic Analysis of the Instep Kick in Youth Soccer Players by," *Journal of Human Kinetics*, vol. 42, no. September, pp. 81–90, 2014.

[36] A. Koizumi, S. Hong, K. Sakamoto, R. Sasaki, and T. Asai, "A study of impact force on modern soccer balls," in *Procedia Engineering*, vol. 72, 2014, pp. 423–428.

[37] G. Barblatt, *Scaling*. Cambridge: Cambridge University Press, 2003.

[38] S. C. Cotter, "A Screening Design for Factorial Experiments with Interactions," *Biometrika*, vol. 66, no. 2, pp. 317–320, 1979.

[39] H. Nunome, M. Lake, A. Georgakis, and L. K. Stergioulas, "Impact phase kinematics of instep kicking in soccer," *Journal of Sports Sciences*, vol. 24, no. 1, pp. 11–22, 2007. [Online]. Available: http://www.tandfonline.com/action/journalInformation?journalCode=rjsp20

[40] A. O. Cerrah, A. R. Soylu, H. Ertan, and A. Lees, "The Effect of Kick Type on the Relationship between Kicking Leg Muscle Activation and Ball Velocity," *J. Sports Sci. Med*, vol. 7, pp. 39–44, 2018. [Online]. Available: http://mjssm.me/?sekcija=article{\&}artid=150

[41] S. P. Broglio, Yan-Ying, J. . Broglio, M. D. Sell, and Timothy C, "The efficacy of soccer headgear," *Journal of Athletic Training*, vol. 38, no. 3, p. 220, 2003.

[42] R. J. Elbin, A. Beatty, T. Covassin, P. Schatz, A. Hydeman, and A. P. Kontos, "A Preliminary Examination of Neurocognitive Performance and Symptoms Following a Bout of Soccer Heading in Athletes Wearing Protective Soccer Headbands," *Research in Sports Medicine*, vol. 23, no. 2, pp. 203–214, 2015. [Online]. Available: https://www.tandfonline.com/action/journalInformation?journalCode=gspm20

[43] J. Auger, J. Markel, N. Leiva, T. M. Talavage, L. J. Leverenz, F. Shen, and E. A. Nauman, "Factors Affecting Peak Impact Force During Headers in Soccer," 2019.

[44] E. Mccuen, D. Svaldi, K. Breedlove, N. Kraz, B. Cummiskey, E. L. Breedlove, J. Traver, K. F. Desmond, R. E. Hannemann, E. Zanath, A. Guerra, L. Leverenz, T. M. Talavage, and E. A. Nauman, "Collegiate women ' s soccer players suffer greater cumulative head impacts than their high school counterparts," *Journal of Biomechanics*, pp. 1–4, 2015. [Online]. Available: http://dx.doi.org/10.1016/j.jbiomech.2015.08.003

[45] T. G. Di Virgilio, A. Hunter, L. Wilson, W. Stewart, S. Goodall, G. Howatson, D. I. Donaldson, and M. Ietswaart, "Evidence for Acute Electrophysiological and Cognitive Changes Following Routine Soccer Heading-NC-ND license (http://creativecommons.org/licenses/by-nc-nd/4.0/)," *EBioMedicine*, vol. 13, pp. 66–71, 2016. [Online]. Available: http://dx.doi.org/10.1016/j.ebiom.2016.10.029

[46] D. T. Kirkendall, S. E. Jordan, and W. E. Garrett, "Heading and Head Injuries in Soccer," *Sports Medicine*, vol. 31, no. 5, pp. 369–386, 2001. [Online]. Available: https://link-springer-com.ezproxy.lib.purdue.edu/content/pdf/10.2165{\%}2F00007256-200131050-00006.pdf

[47] M. Teymouri, H. Sadeghi, A. Nabaei, and A. Kasaeian, "The Relationship Between Biomechanical-Anthropometrical Parameters and the Force Exerted on the Head When Heading Free Kicks in Soccer," *Arch Trauma Res*, vol. 1, no. 1, pp. 44–52, 2012. [Online]. Available: https://www.ncbi.nlm.nih.gov/pmc/articles/PMC3955941/pdf/atr-01-44.pdf

[48] C. W. Fuller, A. Junge, and J. Dvorak, "A six year prospective study of the incidence and causes of head and neck injuries in international football," *Br J Sports Med*, vol. 39, no. 1, pp. i3–i9, 2005. [Online]. Available: www.bjsportmed.com

[49] S. Delaney, V. Puni, and F. Rouah, "Mechanisms of Injury for Concussions in University Football, Ice Hockey and Soccer: A Pilot Study," *Clinical Journal of Sport Medicine*, vol. 16, no. 2, pp. 162–165, 2006. [Online]. Available: https://oce-ovid-com.ezproxy.lib.purdue.edu/article/00042752-200603000-00013/HTML

[50] M. Tarini, N. Pietroni, P. Cignoni, D. Panozzo, and E. Puppo, "Practical Quad Mesh Simplification," *Compute Graphics Forum*, vol. 29, no. 2, pp. 129–136, 2010.

[51] S.-J. Park, "Carbon Fibers." Springer Netherlands, 2015. [Online]. Available: http://link.springer.com/10.1007/978-94-017-9478-7

[52] B.-J. Kim, Y. Eom, O. Kato, J. Miyawaki, B. C. Kim, I. Mochida, and S.-H. Yoon, "Preparation of carbon fibers with excellent mechanical properties from isotropic pitches," *Carbon*, vol. 77, pp. 747–755, 2014. [Online]. Available: https://ac-els-cdn-com.ezproxy.lib.purdue.edu/S0008622314005338/1-s2.0-S0008622314005338-main.pdf?{_}tid=b6106e88-c00b-418c-9c27-c2007feefad9{\&}acdnat=1549246743{_}ad5a77f3d03279233a363a2819a129f3

[53] H. Rahmani, H. M. Najafi, S. Saffarzadeh-Matin, and A. Ashori, "Mechanical Properties of Carbon Fiber/Epoxy Composites: Effects of Number of Plies, Fiber Contents, and Angle-Ply Layers," *Polymer Engineering and Science*, vol. 54, no. 11, pp. 2676, 2682, 2014. [Online]. Available: https://onlinelibrary-wiley-com.ezproxy.lib.purdue.edu/doi/pdf/10.1002/pen.23820

[54] Q. Ma, Y. Gu, M. Li, S. Wang, and Z. Zhang, "Effects of surface treating methods of high-strength carbon fibers on interfacial properties of epoxy resin matrix composite," *Applied Surface Science*, vol. 379, pp. 199–205, 2016. [Online]. Available: https://ac.els-cdn.com/S016943321630825X/1-s2.0-S016943321630825X-main.pdf?{_}tid=7bc42a65-1e3c-4dbb-b209-1289ab163f0d{\&}acdnat=1549317642{_}f7e5b55a6b5e8b205fc80fee95c42fc4

[55] M. Avalle, G. Belingardi, and R. Montanini, "Characterization of polymeric structural foams under compressive impact loading by means of energy-absorption diagram," *International Journal of Impact Engineering*, vol. 25, pp. 455–472, 2001. [Online]. Available: https://ac.els-cdn.com/S0734743X00000609/1-s2.0-S0734743X00000609-main.pdf?{_}tid=fa6e2155-22d3-4e94-87c3-d80737a79f2d{\&}acdnat=1549393653{_}cfc8df90430fe0cc34eaf2606ee4fbf7

[56] R. Juntikka and S. Hallstrom, "Selection of Energy Absorbing Materials for Automotive Head Impact Countermeasures," *Cellular Polymers*, vol. 23, no. 5, pp. 263–297, 2004.

[57] B. J. Ramirez and V. Gupta, "Evaluation of novel temperature-stable viscoelastic polyurea foams as helmet liner materials," *Materials and Design*, vol. 137, pp. 298–304, 2018. [Online]. Available: https://doi.org/10.1016/j.matdes.2017.10.037

[58] L. Radziszewski and M. Saga, "Modeling of Non-elastic Properties of Polymeric Foams Used in Sports Helmets," *Procedia Engineering*, vol. 177, pp. 314–317, 2017. [Online]. Available: www.sciencedirect.com

[59] S. G. Kulkarni, X.-L. Gao, S. E. Horner, J. Q. Zheng, and N. V. David, "Ballistic helmets - Their design, materials, and performance against traumatic brain injury," *Composite Structures*, vol. 101, pp. 313–331, 2013. [Online]. Available: http://dx.doi.org/10.1016/j.compstruct.2013.02.014

[60] B. Cummiskey, G. N. Sankaran, K. G. Mciver, D. Shyu, J. Markel, T. M. Talavage, L. Leverenz, J. J. Meyer, D. Adams, and E. A. Nauman, "Quantitative evaluation of impact attenuation by football helmets using a modal impulse hammer," in *Journal of Sports Engineering and Technology*, 2019, pp. 1–11. [Online]. Available: https://journals.sagepub.com/doi/pdf/10.1177/1754337118823603

[61] D. H. Lee, W. I. Lee, and M. K. Kang, "Analysis and minimization of void formation during resin transfer molding process," *Composites Science and Technology*, vol. 66, pp. 3281–3289, 2006. [Online]. Available: https://ac.els-cdn.com/S0266353805002745/1-s2.0-S0266353805002745-main.pdf?{_}tid=ea51bce4-a27f-49e2-8c24-2608848d13b9{\&}acdnat=1549670176{_}088896355d75c926277d338c68877c7e

[62] L. Carlsson, D. Adams, and B. Pipes, *Experimental Characterization of Advanced Composite Materials*, 4th ed. Boca Raton: Taylor & Francis Group, 2014.

[63] DuPont, "Kevlar® aramid fiber." [Online]. Available: http://www.dupont.com/products-and-services/fabrics-fibers-nonwovens/fibers/brands/kevlar.html

[64] M. Cheng, W. Chen, and T. Weerasooriya, "Mechanical Properties of Kevlar ® KM2 Single Fiber," *Journal of Engineering Materials and Technology*, vol. 127, no. 2, pp. 197–203, 2005. [Online]. Available: http://www.asme.org/about-asme/terms-of-use

[65] L. Siedel, "The many uses of Kevlar aramid," *Textile Industries*, vol. 145, p. 36(4), 1981.

[66] K. Flik, S. Lyman, and R. G. Marx, "American Collegiate Men's ice Hockey: An Analysis of Injuries," *The American Journal of Sports Medicine*, vol. 33, no. 2, pp. 183–189, 2005. [Online]. Available: www.ajsm.org/cgi/content/

[67] S. L. Zuckerman, Z. Y. Kerr, A. Yengo-Kahn, E. Wasserman, T. Covassin, and G. S. Solomon, "Epidemiology of Sports-Related Concussion in NCAA Athletes From 2009-2010 to 2013-2014: Incidence, Recurrence, and Mechanisms," *The American Journal of Sports Medicine*, vol. 43, no. 11, pp. 2654–2662, 2015. [Online]. Available: https://journals.sagepub.com/doi/pdf/10.1177/0363546515599634

[68] M. Levy, B. M. Ozgur, C. Berry, H. E. Aryan, and M. L. J. Apuzzo, "Birth and Evolution of the Football Helmet," *Neurosurgery*, vol. 55, no. 656-662, 2004.

[69] P. J. Bishop, R. W. Norman, J. W. Kozey, and P. J. Bishop, "An evaluation of football helmets under impact conditions," *The American Journal of Sports Medicine*, vol. 12, no. 3, pp. 233–236, 1984. [Online]. Available: https://journals-sagepub-com.ezproxy.lib.purdue.edu/doi/pdf/10.1177/036354658401200313

[70] A. Bartsch, E. Benzel, V. Miele, and V. Prakash, "Impact test comparisons of 20th and 21st century American football helmets," *Journal of Neurosurgery*, vol. 116, no. 1, pp. 222–233, 2012. [Online]. Available: https://thejns-org.ezproxy.lib.purdue.edu/view/journals/j-neurosurg/116/1/article-p222.xml

[71] ASTM, "F717-10 Standard Specification for Football Helmets." 2017.

[72] C. Gadd, "Use of a weighted-impulse criterion for estimating lnjury hazard," *SAE Technical Paper 660793*, 1966.

[73] V. N. Poole, K. Abbas, T. E. Shenk, E. L. Breedlove, K. M. Breedlove, M. E. Robinson, L. J. Leverenz, E. A. Nauman, T. M. Talavage, and U. Dydak, "Developmental Neuropsychology MR Spectroscopic Evidence of Brain Injury in the Non-Diagnosed Collision Sport Athlete," *Developmental Neuropsychology*, vol. 39, no. 6, pp. 459–473, 2014. [Online]. Available: https://www.tandfonline.com/action/journalInformation?journalCode=hdvn20

[74] L. Wei and J. Griffin, "THE PREDICITON OF SEAT TRANSMISSI- BILITY FROM MEASURES OF SEAT IMPEDANCE," *Journal of Sound and Vibration*, vol. 214, no. 1, pp. 121–137, jul 1998. [Online]. Available: https://www-sciencedirect-com.ezproxy.lib.purdue.edu/science/article/pii/S0022460X98915401

[75] D. E. Welcome, R. G. Dong, X. S. Xu, C. Warren, T. W. Mcdowell, and J. Z. Wu, "An examination of the vibration transmissibility of the hand-arm system in three orthogonal directions," *International Journal of Industrial Ergonomics*, vol. 45, pp. 21–34, 2015. [Online]. Available: http://dx.doi.org/10.1016/j.ergon.2014.11.001

[76] R. Deboli, A. Calvo, and C. Preti, "Whole-body vibration: Measurement of horizontal and vertical transmissibility of an agricultural tractor seat," *International Journal of Industrial Ergonomics*, vol. 58, pp. 69–78, 2017. [Online]. Available: http://dx.doi.org/10.1016/j.ergon.2017.02.002

[77] NOCSAE, "Standard Pneumatic Ram Test Method and Equipment Used in Evaluating the Performance Characteristics of Protective Headgear and Face Guards," 2018.